

Determination of robust metallicities for metal-rich red giant branch stars [★]

An application to the globular cluster NGC 6528

C. Liu^{1,2}, G. Ruchti¹, S. Feltzing¹, and F. Primas³

¹ Lund Observatory, Department of Astronomy and Theoretical Physics, Box 43, SE-221 00 Lund, Sweden
e-mail: [cheng, greg, sofia]@astro.lu.se

² Key Lab of Optical Astronomy, National Astronomical Observatories, Chinese Academy of Sciences, A20 Datun Road, Chaoyang, Beijing 100012, China

³ European Southern Observatory, D-85748 Garching, Germany
e-mail: fprimas@eso.org

Received 05 May 2016; accepted 05 January 2017

ABSTRACT

Context. The study of the Milky Way relies on our ability to interpret the light from stars correctly. With the advent of the astrometric ESA mission *Gaia* we will enter a new era where the study of the Milky Way can be undertaken on much larger scales than currently possible. In particular we will be able to obtain full 3D space motions of red giant stars at large distances. This calls for a reinvestigation of how reliably we can determine, e.g., iron abundances in such stars and how well they reproduce those of dwarf stars.

Aims. Here we explore robust ways to determine the iron content of metal-rich giant stars. We aim to understand what biases and shortcomings widely applied methods suffer from.

Methods. In this study we are mainly concerned with standard methods to analyse stellar spectra. This includes the analysis of individual lines to determine stellar parameters, analysis of the broad wings of certain lines (e.g., H α and calcium lines) to determine effective temperature and surface gravity for the stars.

Results. For NGC 6528 we find that [Fe/H] = +0.04 dex with a scatter of $\sigma = 0.07$ dex, which gives an error in the derived mean abundance of 0.02 dex.

Conclusions. Our work has two important conclusions for analysis of metal-rich red giant branch stars. 1) For spectra with S/N below about 35 per reduced pixel [Fe/H] become too high, 2) Determination of T_{eff} using the wings of the H α line results in [Fe/H] values about 0.1 dex higher than if excitational equilibrium is used. The last conclusion is perhaps not surprising as we expect NLTE effect to become more prominent in cooler stars and we can not use the wings of the H α line to determine T_{eff} for the cool stars in our sample. We therefore recommend that in studies of metal-rich red giant stars care needs to be taken to obtain sufficient calibration data in order to be able to also use the cooler stars.

Key words. Galaxy: bulge – globular clusters: individual: NGC 6528 – stars: atmospheres – stars: fundamental parameters

1. Introduction

The analysis of spectra of red giant branch stars is problematic. As we progress along the red giant branch upwards, to cooler and lower gravity stars a number of phenomena start appearing more and more strongly in the spectra. In particular, the atomic lines get stronger, causing more blends and the cooler atmospheres allow for the formation of molecules such as TiO, CN, and MgH resulting in strong molecular features. This makes it progressively more and more difficult to find (or define) the continuum in the spectrum. As many methods rely on the identification of the continuum, this causes a problem.

Our main aim with the present investigation is to study how we can, in a robust way, determine the iron abundance for metal-

rich giants, such as those seen in the Galactic bulge and old, metal-rich globular clusters. We are interested in providing a better understanding of the influence on the derived iron abundance from the signal-to-noise ratio (S/N) in the analysed spectra and any influence on the method used to determine the other stellar parameters, e.g., T_{eff} and $\log g$, on the final iron abundance.

Why is this interesting? The study of the Milky Way has in the last couple of decades become a major area in astrophysics. This is due to two influential astrometric missions: the past Hipparcos mission (Perryman et al. 1997) and the current *Gaia* mission (Brown 2013; Perryman et al. 2001, where the first paper describes the concept behind the *Gaia* proposal to the European Space Agency and the second paper gives an overview of, *Gaia* just before launch). The Hipparcos catalogue enabled a new type of studies with determination of accurate velocities and ages for samples consisting of many hundreds of stars near the sun (e.g., Adibekyan et al. 2013, 2012; Bensby et al. 2004, 2014; Fuhrmann 2011; Soubiran & Girard 2005). These studies were done on F and G dwarf stars. However, *Gaia* will provide data of

[★] Based on observations made with the ESO/VLT, at Paranal Observatory, under programme 067.B-0382(A) and on data obtained from the ESO Science Archive Facility under programme 065.L-0340(A), 067.D-0489(A), and 077.B-0327(A) and from the Keck Observatory Archive under programme C53H and C19H.

Table 1. Basic data for NGC 6528

R.A.	Dec.	(m-M)	E(B-V)
18 04 49.64	−30 03 22.6	16.17	0.54

the same quality as Hipparcos for a significantly larger volume of the Milky Way, reaching all the way in to the Galactic bulge. But, the stars available for spectroscopic work will (as today) be the red giant branch stars as these are intrinsically sufficiently bright to be possible to observe with current instrumentation at a distance of 8 kpc. The only option to obtain spectra for dwarf stars in the Galactic bulge is currently to take advantage of microlensing events (e.g., Bensby et al. 2013). This is, however, not an option if we want to study large samples. Thus it remains important to study how we best can determine stellar parameters and elemental abundances of evolved red giant stars in a robust manner. This paper deals with this topic.

The spectroscopic and photometric data *Gaia* benchmark stars and stars in the metal-rich globular cluster NGC 6528 are presented in Sect. 2. Our basic tools and linelist are described in Sect. 3. To determine stellar parameters for red giants we explore different methods and test them on the benchmark stars in Sect. 4. In Sect. 5 we apply our analysis to stars in NGC 6528 and discuss problems in the analysis. In Sect. 6, we determine [Fe/H] for NGC 6528. Section 7 provides our conclusions and discusses future developments.

2. Description of data

2.1. Spectra

2.1.1. Benchmark stars

In order to work out the best analysis techniques for metal-rich cool giant stars we make use of spectra of stars with well-determined stellar parameters, the so called *Gaia* benchmark stars (Heiter et al. 2015a). These have a wealth of high quality data available, in particular they have interferometric observations enabling a direct determination of their radii and effective temperatures (T_{eff}). As we are interested in metal-rich stars, we selected ten red giants which have iron abundances greater than -0.55 dex (Jofré et al. 2014). The ten stars, which have T_{eff} similar to the stars of NGC 6528, are Arcturus, μ Leo, HD107328, β Gem, ϵ Vir, ξ Hya, α Cet, γ Sge, α Tau, and β Ara. Their reference values for the stellar parameters are listed in Table 3.

The fifteen spectra with high S/N (> 250) were taken from the ESO archive and from observations done with NARVAL. The spectra from the ESO archive consist of observations taken with UVES (Dekker et al. 2000) and HARPS (Mayor et al. 2003). The NARVAL spectra are further described in Blanco-Cuaresma et al. (2014), which also gives details on how to retrieve the spectra from their archive. It should be noted that five stars, μ Leo, β Gem, ξ Hya, α Cet, and γ Sge, have one spectrum each, while the rest of stars have two spectra observed in different instruments. For example, the star Arcturus was observed with the NARVAL and UVES spectrographs, while β Ara was observed with the HARPS and UVES spectrographs.

2.1.2. Stars in NGC 6528

The basis for our study of stars in NGC 6528 is our own observations of 7 stars that were observed in 2001. In order to have a statistically significant sample of spectra of red giant stars in NGC 6528 we further searched the ESO and the KECK

archives. In the archive we found spectra of 34 stars that are potential members of NGC 6528. Of these 12 have been observed by UVES on VLT in stand-alone mode, 20 with UVES as part of FLAMES observations, and 2 stars had been observed with HIRES on KECK. Table 2 lists basic information about the stars and observations. There is no overlap between the observations from the different programmes. Below we describe the different data-sets in some detail.

Stars observed with UVES: Our starting data-set consists of observations of seven stars carried out in 2001 at the VLT 8-m telescope using the UVES spectrograph (Dekker et al. 2000) under our program 067.B-0382(A) (PI: S. Feltzing). The stars were selected as members of NGC 6528 based on a proper motion study using high-resolution images and *VI* photometry from *HST* (see Feltzing & Johnson 2002). In the ESO archive we found an additional five stars observed with UVES from programme 065.L-0340(A) and 067.D-0489(A) (PI: D. Minniti). These were all observed in 2000 and 2001, respectively.

The resolution of the observations is 45000 or 55000 in the red arm (480–680 nm) depending on the slit width used (0.8'' or 1.0''). The observations were all done using the standard setup 580 with CD #3. The exposures have been split in order to allow for the removal of cosmic ray hits. The data were reduced using the UVES pipeline (Ballester et al. 2000), including bias, inter-order background subtraction, flat field correction, extraction, and wavelength calibration. All the echelle orders were then merged into a 1D spectrum for each exposure.

In the archive we found 20 stars which are potential members of NGC 6528 from program 077.B-0327(A) (PI: M. Zoccali) which was observed in 2006.

The multi-object optical spectrograph FLAMES (Pasquini et al. 2002) has two parts, one being FLAMES-UVES which has 8 robotic fibers which feed the UVES spectrograph at VLT. The spectra have $R \sim 47000$ and the observations were done with the setup centred at 580 nm (wavelength coverage: 480–680 nm). We reduced the raw frames using the FLAMES-UVES pipeline in a standard way. After all the recipes, which include creating a master bias and the master slit flat-field frame, determining the fiber order table, the wavelength solution, and extracting the science frame, of the pipeline have been executed we subtract the sky background spectrum from the stellar spectra. For FLAMES-UVES the sky background is usually observed by one fiber placed in an empty part of the sky. With the sky background removed, we shifted the sky-subtracted spectra to a heliocentric reference frame making use of the packages *RVS AO* and *DOPCOR* within IRAF¹.

To improve the S/N, we co-added all the UVES spectra of the same star into a single spectrum. The average S/N of the final co-added spectrum for each star was estimated by making use of the *SPLIT* task within IRAF at three short wavelength regions (574.4 – 574.7 nm, 604.7 – 606.3 nm, and 606.8 – 607.6 nm). The S/N is greater than 30 per pixel for most of the spectra (see Table 2).

Stars observed with HIRES: We collected spectra of two red horizontal branch stars (3014 and 3025) from the Keck Observatory archive. The observations were taken with HIRES (Vogt

¹ IRAF is distributed by the National Optical Astronomy Observatory, which is operated by the Association of Universities for Research in Astronomy (AURA) under cooperative agreement with the National Science Foundation.

et al. 1994) at Keck I under the programme C53H and C19H (PI: J. Cohen) in 1999 and 2000, respectively.

Since the HIRES detector is not large enough to yield full spectral coverage, there is a gap (1.0 – 6.0 nm) between any two echelle orders. The raw spectra were reduced using the MAKEE² package. It determines the position of each echelle order, defines the object and background extraction boundaries, optimally extracts a spectrum for each order, and compute wavelength calibrations non-interactively.

We co-added the spectra of each star into one spectrum. The measured mean S/N of the co-added spectra was estimated in the same way as for the UVES spectra (Table 2).

2.2. Additional data for NGC6528

2.2.1. Photometry

In order to estimate good starting values for T_{eff} for our stars we make use of colour-temperature-metallicity relations. To this end we collected near-infrared photometric data from 2MASS (Cutri et al. 2003) and VVV (VISTA Variables in Via Lactea) (Minniti et al. 2010).

The survey area of VVV is fully imaged in five photometric bands: Z, Y, J, H, K_s and 2MASS has imaging in J, H, K_s . VVV goes about 4 magnitudes deeper than 2MASS. However, the larger telescope aperture of VISTA results in saturation for the brightest stars. The saturation magnitude in the VVV photometry occurs at $K_s < 12$. We therefore adopt 2MASS photometry for stars brighter than 12 mag in K_s and we require that the photometric quality flag is AAA, i.e. the best quality. For all other stars we use VISTA photometry.

There is a very small offset between the zero-points of the VVV and 2MASS catalogs. To ensure that all photometry is on the same system we have chosen to transfer the VVV photometry onto the 2MASS photometric system as this is the system most commonly used in the available temperature calibrations. The following zero-point offsets have been applied: $(J_{2\text{mass}} - J_{\text{vvv}}) = 0.029$; $(H_{2\text{mass}} - H_{\text{vvv}}) = -0.039$; $(K_{s,2\text{mass}} - K_{s,\text{vvv}}) = -0.028$ (Gonzalez et al. 2011).

2.2.2. Reddening

Reddening is important for the initial estimate of T_{eff} , but it can also be of interest when discussing the properties of the cluster. Here we make use of the recent reddening maps by Gonzalez et al. (2011, 2012) to estimate the reddening towards our stars.

As the maximum sky resolution of the reddening map is $2'$, we assumed that the stars are subject to the same reddening within a $4' \times 4'$ box. The observed targets are spread in a relatively large area, the total coverage of the dereddened region is $28' \times 28'$ consisting of 49 boxes of $4' \times 4'$. The mean extinction, A_{K_s} , and colour excess, $E(J - K_s)$, are calculated using BEAM³ which uses the extinction law from Cardelli et al. (1989). The adopted coefficients for J, H , and K_s (in the 2MASS passbands) are: $A_J = 1.692E(J - K_s)$, $A_H = 1.054E(J - K_s)$, $A_{K_s} = 0.689E(J - K_s)$. Where $A_{K_s} = 0.689E(B - V)$. The dereddened magnitudes of J, H , and K_s are listed in Table 2.

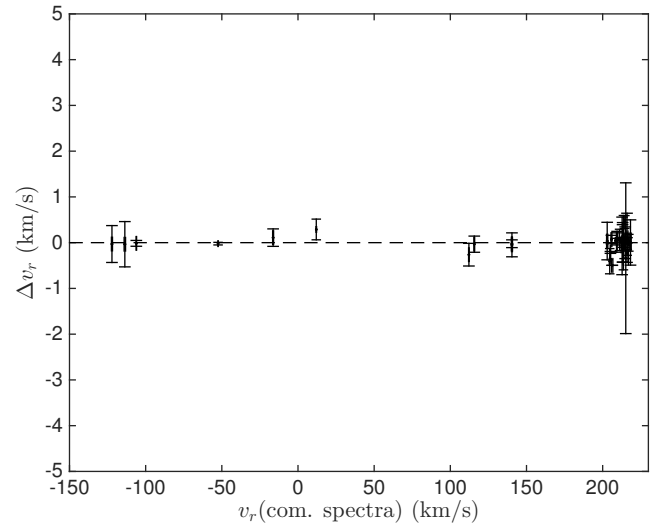


Fig. 1. Comparison of radial velocities for the stars derived from the combined spectrum and from the individual spectra separately and then averaged (see Sect. 2.2.3). The x -axis shows the value derived from the combined spectra whilst the y -axis shows the difference between v_r determined in the two ways. The error-bars for the difference is the coadded errors estimated from IRAF (for the combined spectra) and the σ around the mean for the independent measures. Errors on the x -axis are too small to be seen.

2.2.3. Radial velocities

Radial velocities (v_r) with respect to the Sun were derived using the RVSAO package within IRAF. The XCSAO task cross-correlates a template spectrum with the observed spectrum and reports the velocity difference between the two. Here we used a template spectrum from the radial velocity standard star ϵ Peg. The resolution of the spectrum is similar to that for the spectra of our sample spectra.

Each of our stars have more than one observation (Table 2). The spectra are often taken at different nights and sometimes even months apart. This allows us to derive v_r in two ways, enabling a test of the quality of our results. First we extracted all spectra and corrected them for Earth's motion in order to co-add them. Radial velocities were then determined using these combined spectra. In the other approach we derived the radial velocity for each observation individually. These individual measurements were then averaged and the scatter around the mean was calculated. Typically, the scatter around the mean radial velocities is less than 0.50 km s^{-1} . We find that the two approaches give very similar results (compare Fig. 1).

For unknown reasons, we are unable to recover the radial velocities determined by Carretta et al. (2001) for star 3014 and 3025. Our results are about 50 km s^{-1} larger than the values given by them. As far as we understand we are using the same spectra and same reduction software. In Table 2 we list the value from Carretta et al. (2001). Apart from this difference our derived velocities agree well with those in the literature (see Sect. 2.3).

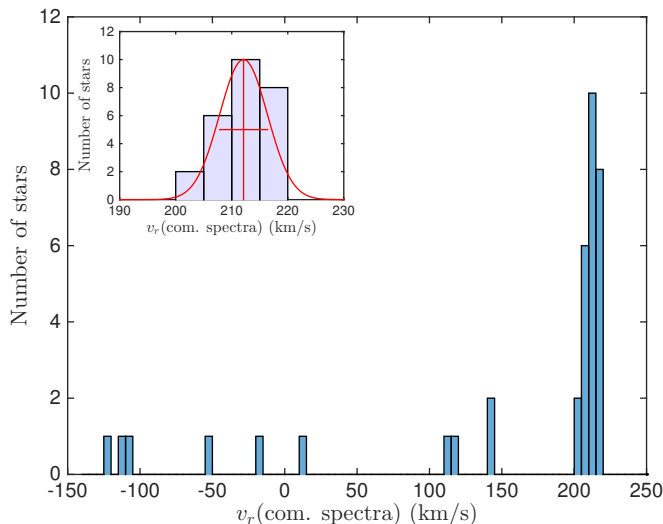


Fig. 2. Distribution of measured heliocentric radial velocities for our program stars. The inset in the top-left corner shows a zoom-in highlighting the velocity distribution of the cluster members fitted by a Gaussian. The red cross indicates the mean (212.1 km s^{-1}) and standard deviation (4.2 km s^{-1}) of the radial velocity for the cluster members.

2.3. Membership

Membership of globular clusters for individual stars is commonly determined using radial velocities (e.g., Simmerer et al. 2013) or proper motions relative to the background and foreground stars (e.g., Zoccali et al. 2001). NGC 6528 has a radial velocity of $\sim 210 \text{ km s}^{-1}$ (Carretta et al. 2001; Zoccali et al. 2004) and a proper motion relative to the background bulge population of $\langle l \rangle = 0.006$ and $\langle b \rangle = 0.044$ arcsec per century (Feltzing & Johnson 2002). This means that radial velocity is the best way to determine membership for this cluster. Using measurements from the luminous stars in globular clusters, as well as their integrated spectra, Pryor & Meylan (1993) determined the velocity dispersions for many globular clusters. They found that typical velocity dispersions in globular clusters is less than 10 km s^{-1} .

Figure 2 shows the distribution of radial velocities for all our stars. There is a clustering of stars just above 200 km s^{-1} . To find the mean velocity and velocity dispersion of NGC 6528, we started by considering stars with a radial velocity in the range $155 - 240 \text{ km s}^{-1}$. For these we calculated the mean and standard deviation (σ) of the radial velocity. We then proceeded to exclude stars more than 3σ from the mean value and the mean and σ were re-calculated. This procedure was iterated until no more stars could be excluded with a 3σ -clipping. This left 26 stars for which we found a mean velocity of 212.1 km s^{-1} and $\sigma = 4.2 \text{ km s}^{-1}$. Our velocity dispersion is in good agreement with the value of 4.0 km s^{-1} measured by Carretta et al. (2001).

3. Linelist and analysis tool

3.1. Line list

To assemble the line list we made use of several sources. For iron we selected 106 clean lines between 470 nm and 690 nm from

Tsantaki et al. (2013), Den Hartog et al. (2014), and the linelist compiled for the *Gaia*-ESO survey (Heiter et al., in prep. and references therein)(see also, Heiter et al. 2015b). In particular, we selected 90 Fe I and 16 Fe II lines. All our lines were examined in the spectra of the Sun and ξ Hya. ξ Hya is a relatively cool and metal-rich star with stellar parameters similar to those in our sample of stars in NGC 6528 and stars in the Galactic bulge (compare values in Table 4). Firstly, these two spectra were used to check that the lines are clean and possible to analyse in metal-rich giant stars. Secondly, the equivalent width (EW) of lines in the two stars were measured. Because the strong lines are sensitive to the selection of the microturbulent velocity (Fulbright et al. 2006) and might suffer from the effects of improper modeling of the outer layers in stellar atmosphere models (McWilliam et al. 1995), all lines with EWs higher than 130 mÅ were removed from our line list.

As cool and metal-rich stars have more molecular lines than warmer stars, we make an extra check to make sure that our lines are not blended by molecules. For this check, we used the spectrum synthetic program (see described in 3.2) and the complete VALD (Kupka et al. 1999, 2000, see also references in the database) line list containing all metal and molecular lines to compute a synthetic spectrum. To generate a spectrum of a cool and metal-rich giant, the typical stellar parameters ($T_{\text{eff}} = 4500 \text{ K}$, $\log g = 2.0$, $[\text{Fe}/\text{H}] = +0.1$ dex) were interpolated in the MARCS model atmospheres (Gustafsson et al. 2008). We examined all the lines by eye and found that most of them are free of TiO, CN, C2, and MgH within 0.2 mÅ of the center of the Fe line. Sixteen Fe lines might suffer a weak contamination from the CN lines. This suggests that our final measured stellar parameters and abundance should not have a large systematic errors caused by the blending of molecular lines.

The oscillator strength ($\log gf$) for the $\text{H}\alpha$ line is adopted from the VALD database. The atomic data for the Ca I lines are taken from Smith & Raggett (1981), apart from the $\log gf$ values for Ca I 612.2 and 616.2 nm, which are from Aldenius et al. (2009).

The full list of lines, including references to atomic data, can be found in the on-line Appendix B (Table B.1).

3.2. Spectral analysis – SME

We use Spectroscopy Made Easy (SME, Valenti & Fischer 2005; Valenti & Piskunov 1996) to determine the stellar parameters by comparing synthetic spectra with observed spectra. SME uses the Levenberg-Marquardt (LM) algorithm to optimize stellar parameters by fitting observed spectra with synthetic spectra. The LM algorithm combines gradient search and linearization methods to determine parameter values that yield a chi-square (χ^2) value close to the minimum. Stellar parameters and atomic line data are required to generate a synthetic spectrum. In addition to specified narrow wavelength segments of the observed spectrum, SME requires line masks in order to compare with synthetic spectrum and determine velocity shifts, and continuum masks that are used to normalize the spectral segments. The homogeneous segments and masks are created to fit all of our solar sibling candidates.

SME needs input values for T_{eff} , $\log g$, $[\text{Fe}/\text{H}]$, microturbulence (v_{mic}), macroturbulence (v_{mac}), and rotational velocity ($v \sin i$). Given initial stellar parameters, the model atmospheres are interpolated in the precomputed MARCS model atmosphere grid, which has standard composition of elemental abundances. We then configured SME to fit each stellar spectrum by adjust-

² http://www.astro.caltech.edu/tb/ipac_staff/tab/makee/index.html

³ <http://mill.astro.puc.cl/BEAM/calculator.php>

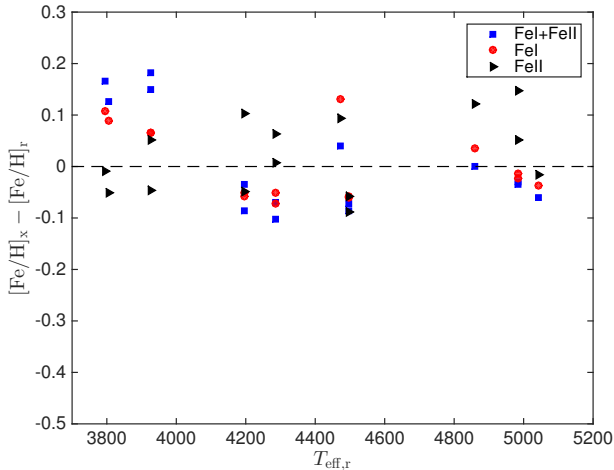


Fig. 3. Test of the ability of our linelist to reproduce the reference $[\text{Fe}/\text{H}]$ for the *Gaia* benchmark stars. The y -axis shows the difference between the value we derive, using the reference T_{eff} and $\log g$ but our own linelist and SME, and the reference value. We derived $[\text{Fe}/\text{H}]$ in three ways: using both Fe I and Fe II lines (blue filled squares), using only Fe I lines (red filled circles), and using only Fe II lines (black filled triangles). The stars can be identified using the T_{eff} values which are given on the x -axis. For some of the stars we have more than one spectrum. Results for both are shown in the plot.

ing the free parameters (see Sect. 4). The convergence is (likely) speedier if we start with realistic initial values. However, it should be noted that SME is capable of converging to the correct values also if we start from initial values that are far off from the correct ones (Daniel Adén, *priv.comm.*, tests for the *Gaia*-ESO Survey).

3.2.1. Can our line list reproduce $[\text{Fe}/\text{H}]$ for stars with known metallicities?

Before starting our investigation, we first checked how well our set-up and linelist reproduces the reference values for $[\text{Fe}/\text{H}]$ for the benchmark stars.

To this end we analysed the spectra fixing T_{eff} and $\log g$ to the recommended values (Table 3). We did three sets of analysis: one where both Fe I and Fe II lines were fitted, one where only Fe I lines were fitted, and one where only Fe II lines were fitted. In each case all lines were all fitted simultaneously.

The results are shown in Fig. 3. We find that when we fit Fe I and Fe II lines simultaneously the difference between our values and the recommended values is 0.01 dex with a σ of 0.10 dex. Figure 3 shows that it is the coolest stars that drives the size of the scatter, whilst the warmer stars have a smaller difference. When we fit only the Fe I lines the difference is 0.01 dex with a σ of 0.07 dex, and when we analyse the Fe II lines only we find a difference of 0.03 dex with a σ of 0.07 dex. There are no discernible trends with T_{eff} , although there is a weak indication that Fe II lines do a better job in reproducing the reference values for the coolest stars (α Cet, γ Sge, and α Tau) while in the warmest stars (β Gem, ϵ Vir, and ξ Hya) Fe I lines appear to do a much better job than the Fe II lines. However, the trend is weak and more data would be needed to draw a firm conclusion regarding if certain species are better at a certain temperature range for these types of stars.

This comparison shows that our line data and method of analysing the iron lines (assuming all other parameters to be known) is fully compatible with those in Jofré et al. (2014) who has established the reference values for the *Gaia* benchmark stars.

4. Looking for a robust method to determine $[\text{Fe}/\text{H}]$ for metal-rich red giant stars from optical spectra

4.1. Methods to derive effective temperature

Effective temperatures can be derived from stellar spectra using several methods. Fe I is the most common ion in terms of lines in the optical spectrum. As lines arising from the Fe I ion have a wide range of line strengths as well as excitation potentials it is in principle straightforward to determine T_{eff} for the star by requiring Fe I lines with differing excitation potentials to produce the same iron abundances (e.g., Edvardsson et al. 1993). This analysis rests on the assumption of local thermal equilibrium (LTE). However, several studies suggest that this assumption does not necessarily hold (e.g., Fuhrmann 1998; Mashonkina et al. 2011; Ruchti et al. 2013; Thévenin & Idiart 1999). Recently, NLTE calculations, e.g., from Bergemann et al. (2012), have been included into some studies (e.g., Ruchti et al. 2013). However, at solar metallicities the difference between LTE and NLTE results for Fe I tend to be very small for metal-rich stars (Ruchti et al. 2013) and we can thus neglect them here. Determination of the iron abundance is a by-product when T_{eff} is derived in this way and errors in the T_{eff} and iron abundance must correlate.

Another method to derive T_{eff} is to use the strong hydrogen lines present in stellar spectra as these lines change rapidly in strength as a function of T_{eff} . These lines also have no gravity dependence in cool stars. Most commonly, T_{eff} is derived from the synthesis of the extended wings of the H α and H β lines (e.g., Barklem et al. 2002; Ruchti et al. 2013). This makes them very useful for determining the temperature for stars with $T_{\text{eff}} < 8000$ K (Gray 2005). With this method iron must be determined independently and hence the errors are not correlated.

Another approach is to use line-depth ratios to derive T_{eff} (Gray 1994). One advantage of using line-depth ratios is that these do not depend on the metallicity of the star. In the visible spectral range, unblended Si, Ti, V, Cr, Fe and Ni line-depth ratios can be used to estimate T_{eff} . There are not many applications of this method in the literature, but Kovtyukh & Gorlova (2000) illustrated that the line-depth ratios are powerful indicators of T_{eff} at least for supergiants. We will not further explore this method here.

Finally, we can use calibration of stellar photometry to derive T_{eff} from a colour index, such as $(B - V)_0$ (see, e.g., González Hernández & Bonifacio 2009). This method has its limitations. For example, for stars in the Galactic bulge or in the plane of the Galaxy the photometric approach is hampered by the poorly determined reddening of individual stellar colours. Although this method is not very dependable for bulge stars, thanks to the large reddening along the line-of-sight, it nevertheless provides useful starting values for our analysis.

4.2. Methods to derive surface gravity

It is common to measure $\log g$ by imposing ionization equilibrium which means that we require Fe I and Fe II lines to produce

the same abundance⁴. Fe II lines can be weak and they are not as numerous as the Fe I lines. This method thus requires high quality spectra with large wavelength coverage. As discussed above (Sect. 4.1) Fe I lines can be susceptible to departures from LTE. This is not true for Fe II lines. Which means that ionizational balance can be influenced by departures from LTE. Determination of the iron abundance is a by-product of this method and errors in $\log g$ and $[\text{Fe}/\text{H}]$ must correlate.

Several lines show strongly pressure-broadened wings in the spectra of cooler stars. This means that the surface gravity of late-type stars can be determined from analysis of these lines. Lines that have pressure broadened wings include the Mg I b lines at 516.7, 517.2, 518.3 nm, the Na I D lines at 588.9 and 589.5 nm, and the Ca I lines at 612.2, 616.2, and 643.9 nm (see, e.g., Bonnell & Bell 1993; Edvardsson 1988; Fuhrmann et al. 1997). The analysis of the wings of these strong lines require that the elemental abundance of the element the line is arising from is also determined, from other lines than the one used to derive $\log g$. This means that errors in $\log g$ and the abundance of that element correlate.

Finally, when we have independent measurements of T_{eff} and metallicity, $\log g$ can be derived through isochrone fitting (see, e.g., Sozzetti et al. 2007). We will not further explore this method here.

4.3. Determining stellar parameters

In Sects. 4.1 and 4.2 we discussed various ways to determine T_{eff} and $\log g$. Although this is not an exhaustive summary, combining the various ways to derive T_{eff} and $\log g$ still leads to quite a few possible combinations. Here we will explore the following combinations:

Method 1: In this method we only use Fe I and Fe II lines to constrain all stellar parameters (i.e., excitation and ionizational equilibria are imposed).

Method 2: In this method we use the H α line to constrain T_{eff} , the strong Ca I lines to constrain $\log g$, and Fe I lines to derive the iron abundance.

Method 3: In this method we use the H α line to constrain T_{eff} , the strong Ca I lines to constrain $\log g$, and Fe II lines to derive the iron abundance.

While in Method 1 all parameters are correlated, Method 2 and 3 aim at breaking these degeneracies by using separate measures for each of the three main parameters. We did not attempt to use the Mg I b and Na I D lines as these are too blended by the atomic and molecular lines to determine $\log g$ from them in metal-rich giant stars as we are interested in here. For cool giants with $T_{\text{eff}} < 4400$ K, we further found that the wings of the H α line almost vanished (see also Appendix C). This lead us to modify Method 2 to be able to include also such stars in our study (see Sect. 4.3.2).

In addition to T_{eff} , $\log g$, and $[\text{Fe}/\text{H}]$ a spectroscopic analysis normally calls for the determination of a few other parameters; microturbulence (v_{mic}), macroturbulence (v_{mac}), and rotational velocity ($v \sin i$).

Microturbulence and macroturbulence can either be derived from the spectrum itself or obtained from a calibration, such as

⁴ In principle other elements can also be used (e.g., Ti). However, there are only a few elements that have lines arising from both the neutral and singly ionised variety of the atom that are observable in the optical part of the spectrum. In those cases, often one of the ions has very few or very weak lines.

those in Jofré et al. (2014). Rotational velocities of red giants and horizontal branch stars are typically small ($v \sin i < 5$ km s⁻¹), therefore a good assumption is to set $v \sin i$ to 1 km s⁻¹. Which is what we do for the rest of this paper. We note that there is often a degeneracy between $v \sin i$ and v_{mac} which is hard to break in the analysis. For the type of study presented here – where the aim is to get the best measure of $[\text{Fe}/\text{H}]$ – the exact values of these two parameters is of less relevance to the final outcome of the investigation and we can allow them to be degenerate. This implies that in this study we can regard them (together) as nuisance necessary to fit but not necessarily giving physical insight in to the star.

To test the three methods we adopted ten benchmark stars (see Heiter et al. 2015a; Jofré et al. 2014, and Sect. 2.1.1).

4.3.1. Method 1: Fe I and Fe II lines

In this method we fit all free parameters simultaneously by comparing the observed spectrum with a synthetic one for short regions around the Fe I and Fe II lines. It should be mentioned that the method is more commonly performed with equivalent widths in the literatures (e.g., Bensby et al. 2003). This method is speedier if we start with realistic initial values for stellar parameters (see also Sect. 3.2). For the benchmark stars, their recommended values are used as the initial input, however, experience shows that the exact values are unimportant to achieve convergence. An initial value for v_{mic} was obtained using the relation given in Jofré et al. (2014). The initial v_{mac} value was set to 5.0 km s⁻¹ for all stars.

All parameters are simultaneously fitted inside SME. As SME strives to fit all lines equally well this is in effect the same as requiring ionizational and excitational equilibrium – hence, all parameters are determined simultaneously. The method differs slightly from its most common implementation in the literature where an iterative scheme is employed and one parameters is varied in each step (see, e.g., Drake 1991; Drake & Smith 1991, and discussions therein). Instead, the usage of SME in fully free mode is more akin to the method used in Feltzing et al. (2009) where the parameter space is searched (by hand) for a best fit to all criteria simultaneously.

4.3.2. Method 2: H α , Ca, and Fe I lines

To break the degeneracy between the different parameters we use different spectral indicators for each of the main stellar parameters. This method requires a set of initial parameters to get started. These could be obtained in different ways (e.g., from photometry). For this test we take the parameters obtained in Method 1 as initial input.

Method 2: For warm giants ($T_{\text{eff}} > 4400$ K), the following steps are used:

1. A set of parameters as initial input;
2. Fit the wings of H α to derive T_{eff} , while the other parameters are kept fixed;
3. Fit the wings of the three strong Ca I lines (λ 612.2, 616.2, and 643.9 nm) to determine $\log g$. To break the degeneracy of $\log g$ and Ca abundance, several weak Ca I lines are also fitted at the same time;
4. Derive $[\text{Fe}/\text{H}]$ from the Fe I lines by setting both v_{mic} and v_{mac} free, while the other parameters are kept fixed at the values derived in the steps above;
5. Repeat steps 2 to 4 with updated parameters until all five parameters reach convergence.

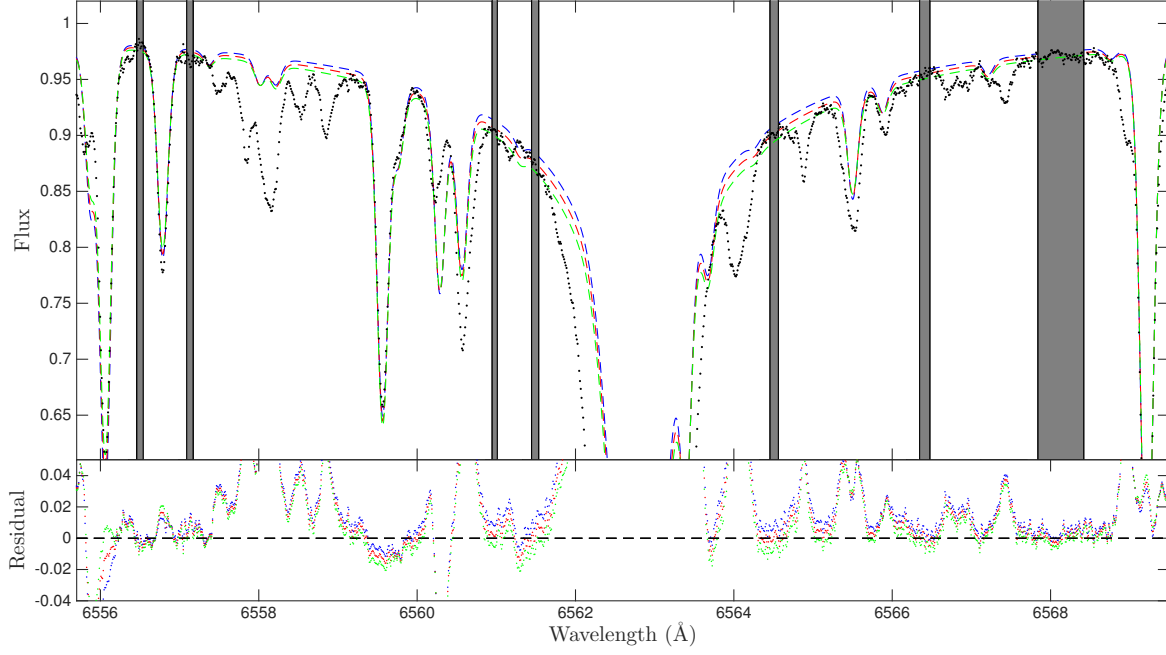


Fig. 4. Comparison of synthetic spectra with the wings of H α line in ϵ Vir. The middle synthetic spectrum (in red) shows the best fit. The other two synthetic spectra (blue and green) indicate the shape of the wings when T_{eff} is changed according to our estimated uncertainty (here 50 K). The gray areas mark the regions used to evaluate the goodness of the fit. Note that these are relatively narrow since the spectrum has very little clean “line continuum” thanks to the cool temperature of the star, which results in many lines being present in the spectrum.

Table 3. Stellar parameters for the *Gaia* benchmark stars. Columns 2 to 4 give the reference values for the stellar parameters. Columns 5 till 11 list our results, derived using Method 2 and Modified Method 2 (Sect. 4.3.2).

Name	Reference values			Results from Method 2						
	$T_{\text{eff},r}$ (K)	$\log g_r$	$[\text{Fe}/\text{H}]_r$ (dex)	T_{eff} (K)	$\sigma_{T_{\text{eff}}}$ (K)	$\log g$	$[\text{Fe}/\text{H}]$ (dex)	$\sigma_{[\text{Fe}/\text{H}]}$ (dex)	V_{mic} (km s $^{-1}$)	V_{mac} (km s $^{-1}$)
μ Leo HD107328	4474	2.51	0.25	4513	100	2.50	0.31	0.08	1.5	4.8
	4496	2.09	−0.33	4484	50	2.00	−0.48	0.09	1.8	4.4
	—	—	—	4483	50	2.01	−0.45	0.06	1.8	5.4
β Gem	4858	2.90	0.13	4846	50	2.89	0.11	0.08	1.2	4.2
ϵ Vir	4983	2.77	0.15	5056	50	2.84	0.16	0.08	1.5	5.5
	—	—	—	5055	50	2.80	0.17	0.08	1.5	5.7
ξ Hya	5044	2.87	0.16	4991	50	2.96	0.10	0.08	1.4	6.1
Results from Modified Method 2										
Arcturus	4286	1.64	−0.52	4305	100	1.69	−0.58	0.09	1.7	5.4
	—	—	—	4321	100	1.63	−0.61	0.09	1.7	5.2
α Cet	3796	0.68	−0.45	3888	100	0.72	−0.43	0.12	1.6	8.9
γ Sge	3807	1.05	−0.17	3988	100	0.96	−0.17	0.09	1.6	6.6
α Tau	3927	1.11	−0.37	3910	100	1.12	−0.27	0.11	1.4	5.7
	—	—	—	3930	100	1.10	−0.28	0.10	1.4	6.1
β Ara	4197	1.05	−0.05	4250	100	1.03	−0.17	0.08	3.0	10.4
	—	—	—	4277	100	1.26	−0.13	0.08	3.0	9.8

Notes. The first column gives the name of the star. The second and third columns give the recommended effective temperature and surface gravity obtained from Heiter et al. (2015a), while the recommended metallicity from Jofré et al. (2014) is listed in the column 4. For some stars we have two spectra from different instruments (see details in Sect. 2.1.1). The second spectrum is indicated by a dash in these three columns. The following seven columns give our results.

For step 2 a number of synthetic spectra are generated and their fit is evaluated using the spectral regions indicated in Fig. 4. Further examples can be found in the on-line material in Appendix C.

In Step 3 the three strong Ca I lines are simultaneously fitted. It would be possible to fit them each individually instead. A discussion of the merits of the different approaches can be found in the on-line material in Appendix D.

Step 5 require us to decide when a given parameter has converged. For the current work the following convergence criteria were applied: between two iterations the differences should be $\Delta T_{\text{eff}} < 50$ K for most stars, but for stars with very high S/N -ratios we required < 20 K, $\Delta \log g < 0.05$ dex, and $\Delta [\text{Fe}/\text{H}] < 0.05$ dex.

As mentioned, it is not feasible to measure T_{eff} from the $H\alpha$ line for the cooler giants ($T_{\text{eff}} < 4400$ K). Therefore, the only option is to derive T_{eff} using Fe I lines (excitational equilibrium) rather than the wings of the $H\alpha$ line for these stars. However, this re-introduces a degeneracy between T_{eff} and $[\text{Fe}/\text{H}]$. We are still able to use the three strong Ca I lines to determine $\log g$.

Modified Method 2: For cool giants ($T_{\text{eff}} < 4400$ K, the following steps are used:

1. A set of parameters as initial input;
2. Fit the wings of the three strong Ca I lines (λ 612.22, 616.22, and 643.91 nm) to determine $\log g$. To break the degeneracy of $\log g$ and Ca abundance, several weak Ca I lines are also fitted at the same time;
3. Setting both v_{mic} and v_{mac} free while keeping $\log g$ fixed, we only fit Fe I lines to determine T_{eff} and $[\text{Fe}/\text{H}]$ at the same time;
4. Repeat steps 2 to 3 with updated parameters until all five parameters converge.

4.3.3. Method 3: $H\alpha$, Ca, and Fe II lines

Since the only difference between Method 3 and Method 2 is that we use Fe II rather than Fe I lines, the atmospheric parameters are measured making use of the same iterative process described in Sect. 4.3.2 by changing from Fe I line to Fe II lines.

For Modified Method 2 we did make use of excitation equilibrium using the Fe I lines. However, the number of Fe II lines available is much fewer than Fe I lines and they do not cover a large enough range in excitation potential for us to try to determine T_{eff} from excitation equilibrium. Method 3 is thus only implemented for warm giants ($T_{\text{eff}} > 4400$ K).

4.4. Discussion and error estimates

We now proceed to compare our results for the ten benchmark stars derived using the three methods. A comparison is shown in Fig. 5 and the stellar parameters obtained using Method 2 and Modified Method 2 are listed Table 3. In particular we find ⁵:

Method 1 $\Delta T_{\text{eff}} = 56$ K ($\sigma=79$), $\Delta \log g = -0.04$ ($\sigma=0.20$), and $\Delta[\text{Fe}/\text{H}] = 0.03$ dex ($\sigma=0.11$);

Method 2 $\Delta T_{\text{eff}} = 35$ K ($\sigma=54$), $\Delta \log g = 0.02$ ($\sigma=0.07$), and $\Delta[\text{Fe}/\text{H}] = -0.03$ dex ($\sigma=0.08$);

Method 3 $\Delta T_{\text{eff}} = 19$ K ($\sigma=53$), $\Delta \log g = -0.03$ ($\sigma=0.08$), and $\Delta[\text{Fe}/\text{H}] = 0.04$ dex ($\sigma=0.04$) (**warm giants only**).

Of the three methods method 1 clearly performs the least well. It is noticeable that the scatter in all three stellar parameters are quite a bit higher for this method than for the other two. The offsets are also somewhat larger. From Fig. 5 we see that there is no particular trend in ΔT_{eff} , $\Delta \log g$, and $\Delta[\text{Fe}/\text{H}]$ as a function of T_{eff} . This is reassuring as it indicates that our methods do not have hidden trends in them and that the estimated scatters can be trusted.

Method 3 suffers from the shortcoming that it can not be applied to cooler giants ($T_{\text{eff}} < 4400$ K). This is a severe limitation for the study of globular clusters and field giants in the Galactic bulge. To study the metallicity distributions, we would therefore

⁵ For these estimates we excluded the star HD 107328 as the $[\text{Fe}/\text{H}]$ for that star is very different, and we do not have a straightforward answer to this discrepancy.

recommend Method 2 as providing a sound basis for an analysis of a large sample of stars. It is reassuring that this method not only gives good metallicity estimates but also reliable stellar parameters in general.

The uncertainty in T_{eff} can be estimated by inspecting the comparison of synthetic spectra with the observed spectrum. This is relatively straightforward for the high S/N and high resolution spectra we have for the *Gaia* benchmark stars. We found that the typical uncertainty in T_{eff} is about 50 K for most of the warm giants. One example, ϵ Vir, is shown in Fig. 4. For $\log g$, we found that for most stars the typical uncertainty is around 0.10 dex (see more details in Appendix D).

For $[\text{Fe}/\text{H}]$ we calculate the error in the mean by using the iron abundance from each iron line individually (remember that the parameters are decoupled in this method). Calculating the formal error in the mean we find errors typically around 0.02 dex, whilst σ is just below 0.1 dex (see Table 3).

For the benchmark stars, the typical uncertainties in the recommended T_{eff} and $\log g$ are about 60 K and 0.10 dex (Heiter et al. 2015a), respectively. The scatter in T_{eff} and $\log g$ around the recommended values for the benchmark stars found in this study is comparable with the typical uncertainties of the recommended stellar parameters. There is a very small offset between the recommended $[\text{Fe}/\text{H}]$ and our results when using Method 2. The typical uncertainty in the recommended $[\text{Fe}/\text{H}]$ is comparable to what we find (< 0.02 dex, Jofré et al. 2014).

4.5. How much do the results depend on the S/N in the spectra?

Our tests of different methods have relied on the analysis of high S/N spectra of the metal-rich, cool giants in *Gaia* benchmark sample. Clearly, a study of for example the Galactic bulge will have spectra of much lower S/N. How will this influence the results? We analyse this in two steps. Firstly we will degrade the spectra for the *Gaia* benchmark stars to mimic that of high quality data for stars in the Galactic bulge and secondly we will make use of the extensive data set of stars in NGC 6528 that we have collected.

To test the dependence of our final results on S/N and resolution we have degraded the spectra for the ten benchmark stars and re-analysed them. We chose 45 000 and 20 000 for the resolution and at three different S/N (25, 35, 45). 20 000 is a resolution that is common for FLAMES-GIRAFFE (used in the *Gaia*-ESO Survey) and the future massively multiplex spectrographs (e.g., WEAVE and 4MOST, Dalton et al. 2014; de Jong et al. 2014, respectively).

Comparing with the results derived from the original spectra we found that $[\text{Fe}/\text{H}]$ is weakly overestimated when the spectra are noisier, but $[\text{Fe}/\text{H}]$ does not depend on the resolution of the spectrum. It should be noted that we did not investigate if the abundances of other elements were unaffected. The iron lines we use are carefully selected to be the cleanest and most easy to analyse, for other elements this may not be true.

5. Applying our analysis to stars in NGC 6528

5.1. Stellar parameters for NGC 6528 stars

Initial T_{eff} for the stars were calculated using the colour- T_{eff} - $[\text{Fe}/\text{H}]$ relation from González Hernández & Bonifacio (2009). As we could not obtain photometric data in the optical for all our stars, the dereddened $J - K_s$ colour is used to calculate the initial estimate of T_{eff} . Following previous studies of the metallicity of

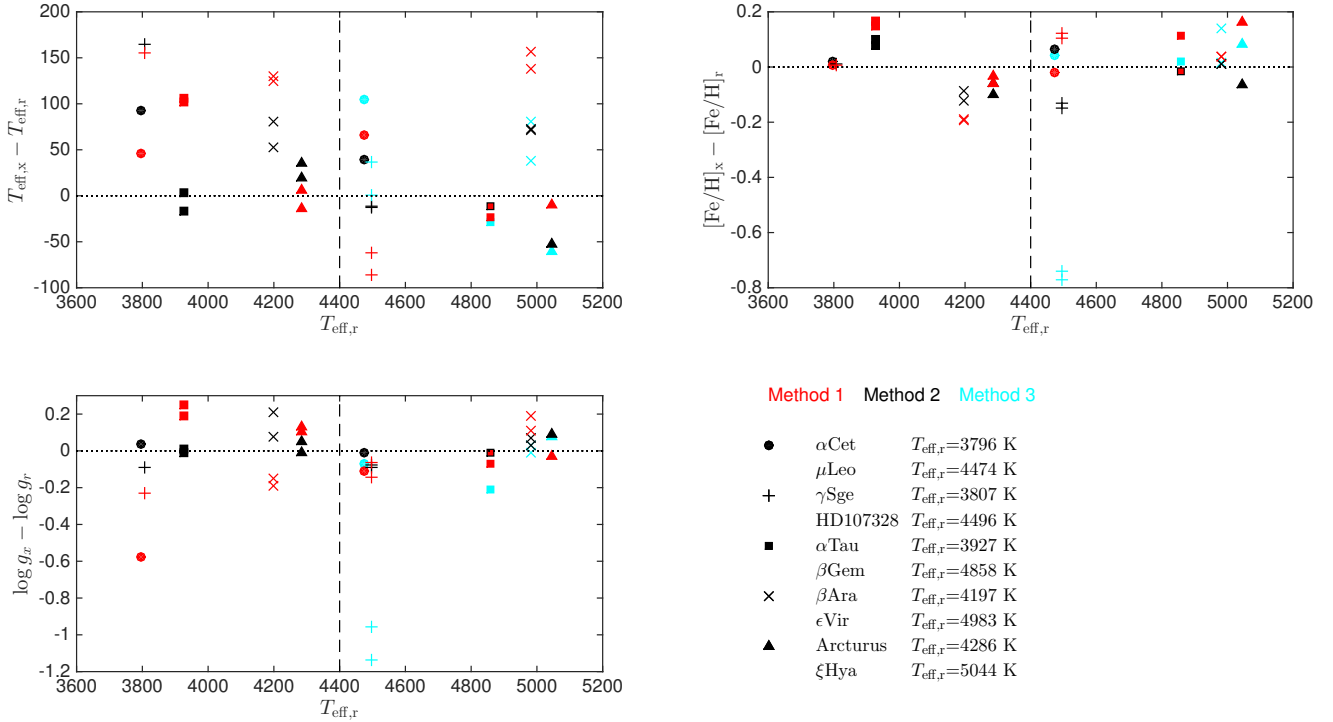


Fig. 5. Comparison of the stellar parameters derived using the three methods discussed in Sects. 4.3.1 till 4.3.3 with the reference values (Table 3). On each y -axis is indicated the difference between the values we have obtained and the reference value (indicated by a subscript "r"). Method 1 is indicated by red symbols, Method 2 by black, and Method 3 is indicated by cyan symbols. Different symbols represent the different stars (as indicated in the figure, note that each symbol represent two stars). They should be easy to identify thanks to their different T_{eff} . Note that some stars have more than one spectrum analysed (see Sect. 2.1.1). The stars can be identified by their recommended T_{eff} which is plotted on the x -axis. The dashed line indicates the separation of "cool" (left) and "warm" (right) giants (see Sect. 4.3.2).

NGC 6528 (e.g., Zoccali et al. 2004), we set $[\text{Fe}/\text{H}] = -0.10$ dex as the initial value for the analysis for all stars. Since most of our stars are either horizontal branch or red clump stars, we simply set the initial $\log g$ to 2.5 dex for warm giants ($T_{\text{eff}} \geq 4400$ K) and 2.0 dex for the cooler. For the analysis we used Method 2 and Modified Method 2, as described in Sect. 4.3.2.

Inspecting the spectrum of star 1-24, we found that most of the lines are asymmetric. Zoccali et al. (2004) found that this star likely is a binary. Our inspection of the spectrum supports this conclusion. The star was removed from our sample.

For stars 61, 66, 68, and 84 we were unable to analyse the spectra as they all have low S/N and in addition the spectra appear to have several unexpected features. These stars were excluded from the analysis.

This leaves us with 29 stars successfully analysed. The results are listed in Table 4. Eight of these stars are not radial velocity members of NGC 6528 (see Sect. 2.3).

5.2. Analysis of a suite of low S/N spectra for stars in NGC 6528

For several of the stars in NGC 6528 we have multiple exposures. This allows us to analyse spectra of different S/N for the same star. Using Method 2 and Modified Method 2 we analysed the actual observed spectra of five stars (star-05, -07, -62, -65 and -67, IDs as in Table 2).

Two of the cluster stars (-62 and -71) have a large number of spectra allowing us to study the results in a more statistical way. For reference value we use the final parameters determined for each star as listed in Table 4.

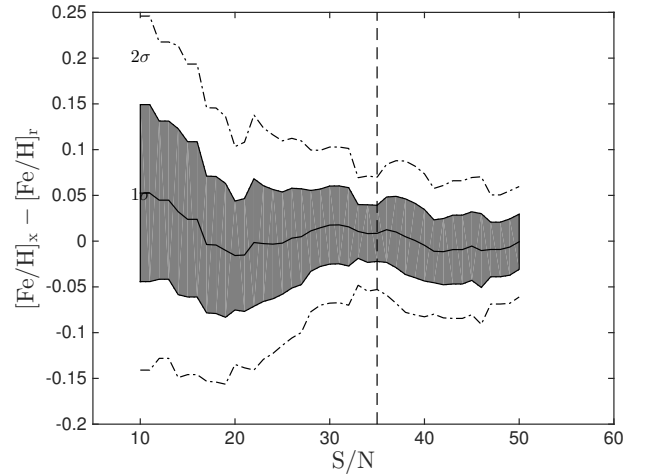


Fig. 6. The difference between $[\text{Fe}/\text{H}]$ derived from spectra of varying S/N (per pixel) for stars in NGC 6528. $[\text{Fe}/\text{H}]_x$ indicates our value measured for each spectrum, while $[\text{Fe}/\text{H}]_r$ indicate the value obtained in Sect. 5.1 for each star. The full line indicated the average difference evaluated as a running average. The shaded region indicates the 1σ difference, while the dashed-dotted line indicates the 2σ difference. Details on individual stars are given in online material in Appendix E. Note that in this figure we do not distinguish between stars for which different methods to derive T_{eff} have been used (compare Fig. 7).

We find that the scatter, for a given star and for the whole sample, increases as we go to spectra with lower and lower S/N.

Table 4. Stellar parameters for the sample stars derived using Method 2.

#	Object	T_{eff} (K)	$\sigma_{T_{\text{eff}}}$ (K)	$\log g$	$\sigma_{\log g}$	[Fe/H]	$\sigma_{[\text{Fe}/\text{H}]}$	V_{mic} (km s ⁻¹)	V_{mac} (km s ⁻¹)	Member
(01)	01	4550	100	2.78	0.02	0.40	0.12	1.8	4.2	N
(02)	02	6042	50	4.51	0.05	0.03	0.04	1.1	8.2	N
(03)	03	4029	100	1.23	0.15	-0.15	0.12	1.5	5.3	Y
(04)	04	4304	100	1.52	0.15	0.04	0.11	1.4	5.3	Y
(05)	05	4277	100	1.95	0.11	0.01	0.10	1.5	4.5	Y
(06)	06	4623	100	1.98	0.08	-0.04	0.14	1.9	6.8	Y
(07)	07	4776	100	2.50	0.09	0.03	0.08	1.7	6.1	Y
(08)	1-02	4258	100	1.67	0.12	0.05	0.09	1.3	9.8	Y
(09)	1-16	4640	100	2.56	0.14	-0.02	0.09	1.5	7.1	Y
(11)	1-36	4337	100	2.14	0.08	-0.08	0.11	1.7	4.8	Y
(12)	1-42	4125	100	1.39	0.19	0.09	0.14	0.8	7.8	Y
(13)	60	4289	100	2.08	0.09	-0.07	0.08	1.7	6.2	Y
(15)	62	3967	100	1.89	0.10	-0.08	0.11	1.8	7.1	Y
(16)	63	3977	100	1.45	0.07	-0.15	0.09	1.8	7.0	Y
(17)	64	4079	100	1.94	0.15	-0.07	0.12	1.7	5.6	Y
(18)	65	4289	100	2.28	0.08	-0.09	0.12	1.9	6.5	Y
(21)	69	4044	100	1.65	0.08	-0.17	0.12	1.7	6.2	Y
(22)	70	4123	100	2.12	0.12	0.09	0.20	1.1	7.3	Y
(23)	71	4560	150	2.64	0.04	0.11	0.08	1.9	7.7	Y
(24)	72	4506	150	2.55	0.04	0.26	0.13	2.2	6.7	N
(25)	73	4702	100	2.62	0.20	-0.02	0.10	2.4	10.9	Y
(26)	75	4153	100	2.00	0.13	0.01	0.10	1.7	4.8	N
(27)	76	4569	150	2.74	0.22	0.43	0.13	2.1	5.4	N
(28)	80	4451	100	2.51	0.05	0.19	0.14	1.7	6.4	Y
(29)	82	4521	100	2.34	0.17	0.40	0.12	2.0	5.2	N
(30)	83	4883	100	2.48	0.21	-0.48	0.07	1.7	5.6	N
(32)	86	3650	150	1.15	0.38	0.03	0.34	1.7	10.0	N
(33)	3014	4797	100	2.21	0.10	0.21	0.11	1.4	6.7	Y
(34)	3025	4877	100	2.02	0.15	0.14	0.09	1.7	15.8	Y

Notes. Column one gives the # from Table 2 in Appendix A, which are also used in the Finding Chart in the same appendix. Column two the original IDs, Columns three to eight lists the derived parameters and their associated errors. Columns nine and ten list the micro and macro turbulences, respectively. "Y" and "N" in the last column indicate if the star is a radial velocity member of NGC 6528 or not.

This is not a new finding, but it is here quantified in detail for, what we believe, is the first time for evolved, metal-rich giant stars. Although the scatter increases as we go to lower S/N the mean value of the measurements more or less reproduces the reference value. At the lowest S/N we find a positive offset (Fig. 6).

Further details are available in the online material in Appendix E.

5.3. Discussion: Do Method 2 and Modified Method 2 produce comparable results?

Unfortunately, the answer to the question posed in the headline of this section is – no. This should perhaps not come as a surprise, but given the results in Sect. 4.4 we would have expected that the results would be relatively similar and no (obvious) systematic differences present. This is, however, not the case.

Figure 7 shows the cumulative distributions of [Fe/H] for stars that are radial velocity members of NGC 6528. We plot the distribution for all stars, but also for stars analysed using Method 2 and Modified Method 2, respectively. Table 5 lists the number of stars in each sub-sample and the average [Fe/H]. Stars analysed using Method 2 are about 0.1 dex more metal-rich than stars analysed with Modified Method 2. The median is similarly off-set. To check that this result does not depend on S/N we also

Table 5. Metallicity estimates for NGC 6528 using different samples. The two first lines in the table gives the results using Method 2 and Modified Method 2 together to analyse the whole sample. The line marked recalibrated presents our final result. Below this, we give the results if the sample is split according to which method is used to analyse the spectra.

	S/N	N_{stars}	$\langle[\text{Fe}/\text{H}]\rangle$	σ	Error
	All	21	0.00	0.10	0.02
	> 35	13	-0.03	0.08	0.02
Recalibrated	> 35	13	0.04	0.07	0.02
Method 2	All	8	0.07	0.10	0.03
	> 35	3	0.04	0.06	0.03
Modified Method 2	All	13	-0.04	0.09	0.02
	> 35	10	-0.05	0.08	0.02

Notes. The first column indicates which methods are included in the average, the second column indicates if all S/N are included or if there is a cut-off, the third column gives the number of stars in the sample, the fifth column lists the average [Fe/H], while columns six and seven lists the associated σ and error-in-the-mean ($\sigma/\sqrt{N_{\text{stars}}}$).

analysed only stars with S/N > 35. Although this results in rather small samples the end-result remains (Fig. 7 b).

We also note that when selecting only stars with S/N > 35 the full sample as well as the two sub-samples all give a lower

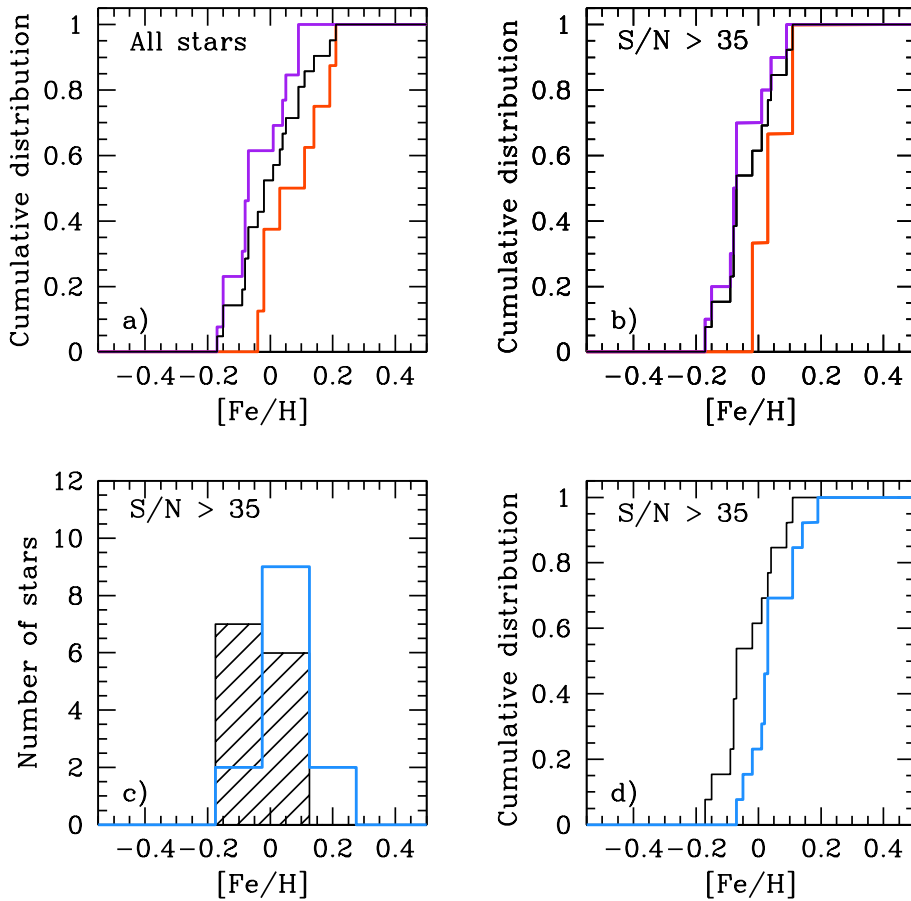


Fig. 7. Distribution of $[\text{Fe}/\text{H}]$ for stars in NGC 6528. **a)** The black line shows the cumulative distribution of $[\text{Fe}/\text{H}]$ for the full sample (21 stars). The orange-red line shows the distribution for stars where we have fitted the wings of H α to determine T_{eff} (Method 2), while the purple line shows the distribution for the stars when we have used excitation equilibrium to determine T_{eff} (Modified Method 2). **b)** The same as in a) but now only for stars with $S/N > 35$. **c)** The black line shows the histogram of $[\text{Fe}/\text{H}]$ for stars in NGC 6528 for all stars with $S/N > 35$, while the blue line shows the result when the offset between the distributions for stars analysed with Method 2 and Modified Method 2 has been accounted for. **d)** The cumulative distribution of $[\text{Fe}/\text{H}]$. The colours are the same as in c).

$[\text{Fe}/\text{H}]$ (by 0.03 dex). This agrees with what we found in the analysis of the noise injected spectra of *Gaia* benchmark stars (see Sects. 4.5 and 5.2).

To summarize, Fig. 6 indicate that the methods are very good at reproducing the final $[\text{Fe}/\text{H}]$ also at relatively low S/N , but below about ~ 35 the errors increase and results in inflated values for $[\text{Fe}/\text{H}]$. However, of greater concern is that the results from the two methods are offset (Fig. 7 a & b).

6. The metallicity of NGC 6528

6.1. Results

Given the results found in Sect. 5.2 and 5.3 defining the iron abundance of the metal-rich globular cluster NGC 6528 requires some care. In Method 2 the degeneracy between T_{eff} and $[\text{Fe}/\text{H}]$ is broken and is thus the most robust method to derive $[\text{Fe}/\text{H}]$ with. Our final result for NGC 6528 will therefore be based on this method. In Fig. 7 (panels c and d) we show the final result when the $[\text{Fe}/\text{H}]$ from Modified Method 2 are calibrated to Method 2 by applying the offset between the two methods to stars analysed with Modified Method 2.

The final sample of stars in NGC 6528 thus contains 3 + 10 stars with $S/N > 35$ (compare Table 5). If we consider these 13 stars which have $S/N > 35$ the mean and standard deviation change to $+0.04$ dex with $\sigma = 0.07$ dex and hence an error in the derived mean abundance of 0.02 dex. This is our best estimate of $[\text{Fe}/\text{H}]$ for NGC 6528.

6.2. Comparison with literature

The spectra of four red horizontal branch stars in NGC 6528 were analyzed by Carretta et al. (2001). They found that the mean $[\text{Fe}/\text{H}]$ for NGC 6528 is 0.07 ± 0.01 dex. Two of these stars (3014 and 3025) are part of our sample. For these stars our $[\text{Fe}/\text{H}]$ are higher than found by Carretta et al. (2001). The difference is particularly large for 3014 for which our value is 0.1 dex higher. The discrepancy between the two results is mainly caused by the difference in T_{eff} . Our T_{eff} is hotter than that of Carretta et al. (2001) by about 150 K, while the $\log g$ s are similar.

Four of our stars (1-16, 1-24, 1-36, and 1-42) were taken from the sample by Zoccali et al. (2004). As discussed above 1-24 is a spectroscopic binary and has been excluded from further analysis. Zoccali et al. (2004) note that 1-16 has a nearby companion. They therefore discarded also this star. As we have a large sample we are less worried about slight contamination of an individual spectrum and have kept the star in the sample.

The $[\text{Fe}/\text{H}]$ determined by us and Zoccali et al. (2004) for 1-36 agree very well. On the other hand, the differences for 1-42 are large. Although the two T_{eff} are very similar there is a difference in the metallicity and gravity of about 0.20 dex. Several possibilities might explain this discrepancy. The most obvious one being that we have different line lists and potentially also different $\log g f$ values for lines in comment ⁶. We have also made use of the latest updates of $\log g f$ -values. We found that the uncertainty in the determined metallicity and gravity is much larger than the typical values, because 1-42 is a cooler giant ($T_{\text{eff}} \sim 4100$ K). Zoccali et al. also found that 1-42 has large

⁶ We can not make a comparison for the two list of iron lines, because Zoccali et al. did not publish their iron line data.

Table 6. Metallicity estimates for NGC 6528 from the literature.

Method	[Fe/H] dex	Ref.
IR abs. at 1.6 μ m	-0.23	1
Low resolution spectra	-0.50 \pm 0.3	2
High resolution spectra (RHBs)	0.07 \pm 0.01	3
RGB morphology indicators	\sim -0.2	4
High resolution spectra (RGs)	-0.10 \pm 0.20	5
High resolution infrared spectra	-0.17 \pm 0.01	6
Photometric calibration	-0.04 \pm 0.27	7

Notes. The numbers in the last column indicate the reference: 1) Origlia et al. (1997); 2) Coelho et al. (2001); 3) Carretta et al. (2001); 4) Momany et al. (2003); 5) Zoccali et al. (2004); 6) Origlia et al. (2005); 7) Calamida et al. (2014)

scatter in iron abundances. We also note that 1-42 has a lower S/N than the other stars from Zoccali et al. (2004). Given that it is also a cool giant and hence analysed with Modified Method 2, it is likely that the results are quite influenced by the deterioration in results below S/N \sim 35 (see also plots in Appendix E). Thus there does not seem to be one single issue that have contributed to the difference but several.

Apart from these two high-resolution studies, several other recent studies are summarized in Table 6. Most of these agree with our results, with the exception of the metallicity derived from a comparison of the low resolution spectra to a grid of synthetic spectra (Coelho et al. 2001).

7. Conclusions and implications for the study of metal-rich stellar populations

With the aim of providing robust measures of [Fe/H] for metal-rich red giant branch stars we have conducted a thorough study of how best to analyse such spectra. We first analysed spectra for a set of so called benchmark stars to see which methods could best reproduce the reference values and secondly we analysed a set of spectra for a metal-rich globular cluster to appraise how well the chosen method fared in a real example with sometimes spectra of poor quality. Our conclusions are the following

- Low S/N in the spectra skews [Fe/H] values to higher values.
- Using excitation equilibrium to determine T_{eff} results in [Fe/H] that are 0.1 dex lower than if we fit the wings of the $H\alpha$ line are used to derive T_{eff} .

These two effects should be taken into account when studying red giant stars in metal-rich stellar populations. In general the best approach would be to ensure large enough S/N in the spectra and only use stars with $T_{\text{eff}} > 4400$ K. However, this might not always be practical or even possible. When cool stars need to be used or when the S/N on average can not be sufficiently high the study should implement a careful approach already at the telescope; a substantial number of warmer stars should be observed at sufficiently high S/N. These stars need not be part of the science sample, but can, for example, be stars in a globular cluster or in the field. In fact, stars in a globular cluster might be preferable as only there will it be straightforward to do the type of comparison that we present in Sect. 5.3

We study the [Fe/H] in the metal-rich and old globular cluster NGC 6528. We find that the best value, taking the various issues summarised above into account, is [Fe/H] = +0.04 dex with $\sigma = 0.07$ dex and hence an error in the derived mean abundance of 0.02 dex.

Acknowledgements. We thank Luca Sbordone who helped us to degrade the original *Gaia* benchmark star spectra to lower resolution and lower S/N. These degraded spectra were used in our tests. This project was supported by the grant No. 621-2011-5042 from The Swedish Research Council. G.R. is funded by the project grant "The New Milky Way" from the Knut and Alice Wallenberg Foundation. This work has made use of the VALD database, operated at Uppsala University, the Institute of Astronomy RAS in Moscow, and the University of Vienna. This research made use of the SIMBAD database, operated at the CDS, Strasbourg, France.

References

- Adibekyan, V. Z., Figueira, P., Santos, N. C., et al. 2013, *A&A*, 554, A44
Adibekyan, V. Z., Sousa, S. G., Santos, N. C., et al. 2012, *A&A*, 545, A32
Aldenius, M., Lundberg, H., & Blackwell-Whitehead, R. 2009, *A&A*, 502, 989
Ballester, P., Modigliani, A., Boitquin, O., et al. 2000, *The Messenger*, 101, 31
Barklem, P. S., Stempels, H. C., Allende Prieto, C., et al. 2002, *A&A*, 385, 951
Bensby, T., Feltzing, S., & Lundström, I. 2003, *A&A*, 410, 527
Bensby, T., Feltzing, S., & Lundström, I. 2004, *A&A*, 415, 155
Bensby, T., Feltzing, S., & Oey, M. S. 2014, *A&A*, 562, A71
Bensby, T., Yee, J. C., Feltzing, S., et al. 2013, *A&A*, 549, A147
Bergemann, M., Lind, K., Collet, R., Magic, Z., & Asplund, M. 2012, *MNRAS*, 427, 27
Blanco-Cuaresma, S., Soubiran, C., Jofré, P., & Heiter, U. 2014, *A&A*, 566, A98
Bonnell, J. T. & Bell, R. A. 1993, *MNRAS*, 264, 334
Brown, A. G. A. 2013, *ArXiv e-prints*
Calamida, A., Bono, G., Lagioia, E. P., et al. 2014, *A&A*, 565, A8
Cardelli, J. A., Clayton, G. C., & Mathis, J. S. 1989, *ApJ*, 345, 245
Carretta, E., Cohen, J. G., Gratton, R. G., & Behr, B. B. 2001, *AJ*, 122, 1469
Coelho, P., Barbuy, B., Perrin, M.-N., et al. 2001, *A&A*, 376, 136
Cutri, R. M., Skrutskie, M. F., van Dyk, S., et al. 2003, *2MASS All Sky Catalog of point sources*.
Dalton, G., Trager, S., Abrams, D. C., et al. 2014, in *Society of Photo-Optical Instrumentation Engineers (SPIE) Conference Series*, Vol. 9147, *Society of Photo-Optical Instrumentation Engineers (SPIE) Conference Series*, 91470L
de Jong, R. S., Barden, S., Bellido-Tirado, O., et al. 2014, in *Society of Photo-Optical Instrumentation Engineers (SPIE) Conference Series*, Vol. 9147, *Society of Photo-Optical Instrumentation Engineers (SPIE) Conference Series*, 91470M
Dekker, H., D’Odorico, S., Kaufer, A., Delabre, B., & Kotzlowski, H. 2000, in *Society of Photo-Optical Instrumentation Engineers (SPIE) Conference Series*, Vol. 4008, *Society of Photo-Optical Instrumentation Engineers (SPIE) Conference Series*, ed. M. Iye & A. F. Moorwood, 534–545
Den Hartog, E. A., Ruffoni, M. P., Lawler, J. E., et al. 2014, *ApJS*, 215, 23
Drake, J. J. 1991, *MNRAS*, 251, 369
Drake, J. J. & Smith, G. 1991, *MNRAS*, 250, 89
Edvardsson, B. 1988, *A&A*, 190, 148
Edvardsson, B., Andersen, J., Gustafsson, B., et al. 1993, *A&A*, 275, 101
Feltzing, S. & Johnson, R. A. 2002, *A&A*, 385, 67
Feltzing, S., Primas, F., & Johnson, R. A. 2009, *A&A*, 493, 913
Fuhrmann, K. 1998, *A&A*, 338, 161
Fuhrmann, K. 2011, *MNRAS*, 414, 2893
Fuhrmann, K., Pfeiffer, M., Frank, C., Reetz, J., & Gehren, T. 1997, *A&A*, 323, 909
Fulbright, J. P., McWilliam, A., & Rich, R. M. 2006, *ApJ*, 636, 821
Gilmore, G., Randich, S., Asplund, M., et al. 2012, *The Messenger*, 147, 25
Gonzalez, O. A., Rejkuba, M., Zoccali, M., Valenti, E., & Minniti, D. 2011, *A&A*, 534, A3
Gonzalez, O. A., Rejkuba, M., Zoccali, M., et al. 2012, *A&A*, 543, A13
González Hernández, J. I. & Bonifacio, P. 2009, *A&A*, 497, 497
Gray, D. F. 1994, *PASP*, 106, 1248
Gray, D. F. 2005, *The Observation and Analysis of Stellar Photospheres*
Gustafsson, B., Edvardsson, B., Eriksson, K., et al. 2008, *A&A*, 486, 951
Harris, W. E. 1996, *AJ*, 112, 1487
Heiter, U., Jofré, P., Gustafsson, B., et al. 2015a, *A&A*, 582, A49
Heiter, U., Lind, K., Asplund, M., et al. 2015b, *Phys. Scr*, 90, 054010
Jofré, P., Heiter, U., Soubiran, C., et al. 2014, *A&A*, 564, A133
Kovtyukh, V. V. & Gorlova, N. I. 2000, *A&A*, 358, 587
Kupka, F., Piskunov, N., Ryabchikova, T. A., Stempels, H. C., & Weiss, W. W. 1999, *A&AS*, 138, 119
Kupka, F. G., Ryabchikova, T. A., Piskunov, N. E., Stempels, H. C., & Weiss, W. W. 2000, *Baltic Astronomy*, 9, 590
Mashonkina, L., Gehren, T., Shi, J.-R., Korn, A. J., & Grupp, F. 2011, *A&A*, 528, A87
Mayor, M., Pepe, F., Queloz, D., et al. 2003, *The Messenger*, 114, 20
McWilliam, A., Preston, G. W., Sneden, C., & Shectman, S. 1995, *AJ*, 109, 2736
Meléndez, J. & Barbuy, B. 2009, *A&A*, 497, 611
Minniti, D., Lucas, P. W., Emerson, J. P., et al. 2010, *New A*, 15, 433

- Momany, Y., Ortolani, S., Held, E. V., et al. 2003, *A&A*, 402, 607
- Origlia, L., Ferraro, F. R., Fusi Pecci, F., & Oliva, E. 1997, *A&A*, 321, 859
- Origlia, L., Valenti, E., Rich, R. M., & Ferraro, F. R. 2005, *MNRAS*, 363, 897
- Pasquini, L., Avila, G., Blecha, A., et al. 2002, *The Messenger*, 110, 1
- Perryman, M. A. C., de Boer, K. S., Gilmore, G., et al. 2001, *A&A*, 369, 339
- Perryman, M. A. C., Lindegren, L., Kovalevsky, J., et al. 1997, *A&A*, 323
- Pryor, C. & Meylan, G. 1993, in *Astronomical Society of the Pacific Conference Series*, Vol. 50, *Structure and Dynamics of Globular Clusters*, ed. S. G. Djorgovski & G. Meylan, 357
- Raassen, A. J. J. & Uylings, P. H. M. 1998, *A&A*, 340, 300
- Ruchti, G. R., Bergemann, M., Serenelli, A., Casagrande, L., & Lind, K. 2013, *MNRAS*, 429, 126
- Simmerer, J., Feltzing, S., & Primas, F. 2013, *A&A*, 556, A58
- Smith, G. & Raggett, D. S. J. 1981, *Journal of Physics B Atomic Molecular Physics*, 14, 4015
- Soubiran, C. & Girard, P. 2005, *A&A*, 438, 139
- Sozzetti, A., Torres, G., Charbonneau, D., et al. 2007, *ApJ*, 664, 1190
- Thévenin, F. & Idiart, T. P. 1999, *ApJ*, 521, 753
- Tsantaki, M., Sousa, S. G., Adibekyan, V. Z., et al. 2013, *A&A*, 555, A150
- Valenti, J. A. & Fischer, D. A. 2005, *ApJS*, 159, 141
- Valenti, J. A. & Piskunov, N. 1996, *A&AS*, 118, 595
- Vogt, S. S., Allen, S. L., Bigelow, B. C., et al. 1994, in *Society of Photo-Optical Instrumentation Engineers (SPIE) Conference Series*, Vol. 2198, *Instrumentation in Astronomy VIII*, ed. D. L. Crawford & E. R. Craine, 362
- Zoccali, M., Barbuy, B., Hill, V., et al. 2004, *A&A*, 423, 507
- Zoccali, M., Renzini, A., Ortolani, S., Bica, E., & Barbuy, B. 2001, *AJ*, 121, 2638

Table 2. Basic information for all stars analysed in this study. The first part of the table contains the data for stars observed with UVES on VLT in stand-alone mode, the second part lists the stars observed with FLAMES-UVES on VLT, and the third part stars observed with HIRES on KECK.

#	Obj.	ID	R.A.	DEC	J_0^a (mag)	H_0^a (mag)	$K_{s,0}^a$ (mag)	v_r (km s ⁻¹)	Date	Exp. (s)	Instrument	S/N ^b
(01)	01	2MASS 18044807-3002301	18 04 48.02	-30 02 30	13.11	12.60	12.46	-52.46±0.18	14.05.01	3x4800	UVES	39
(02)	02	VVV J180448.98-300152.34	18 04 48.98	-30 01 52	16.45	16.09	16.11	12.00±0.45	15.05.01	3x4800	UVES	167
(03)	03	2MASS 18044889-3004066	18 04 48.99	-30 04 07	12.37	11.76	11.58	204.63±0.21	13.06.01	3x4800	UVES	42
(04)	04	2MASS 18044912-3004010	18 04 49.27	-30 04 01				216.65±0.19	14.05.01	2x4800	UVES	41
(05)	05	VVV J180450.06-300159.90	18 04 50.20	-30 01 59	15.58	15.29	15.20	211.68±0.22	19.06.01	3x4800	UVES	55
(06)	06	2MASS 18044721-3002305	18 04 47.17	-30 02 31	13.12	12.66	12.56	211.09±0.29	20.05.01	2x5400	UVES	29
(07)	07	VVV J180447.91-300340.06	18 04 47.78	-30 03 39	13.41	12.89	12.79	216.16±0.23	13.05.01	3x4800	UVES	46
(08)	1-02	VVV J180451.33-300301.99	18 04 51.23	-30 03 03	13.93	13.40	13.35	216.09±0.34	26.06.00	2x4800	UVES	28
(09)	1-16	2MASS 18044953-3003044	18 04 49.60	-30 03 03	12.77	12.21	12.11	208.41±0.21	26.06.00	2x3600	UVES	62
(10)	1-24	2MASS 18045029-3003099	18 04 50.37	-30 03 10	13.18	12.68	12.58	213.62±0.28	26.06.00	4584	UVES	38
(11)	1-36		18 04 50.92	-30 03 48				217.17±0.18	26.06.00	2x5400	UVES	44
(12)	1-42	2MASS 18044900-3003264	18 04 49.11	-30 03 28	12.17	11.48	11.33	214.55±0.26	26.06.00	3x3600	UVES	37
(13)	60	VVV J180448.38-300255.09	18 04 48.36	-30 02 55	12.17	11.61	11.44	206.01±0.26	29.06.06	2x2700	Flames-UVES	39
								206.68±0.23	31.05.06	2x2700	Flames-UVES	
(14)	61	2MASS 18044812-3003082	18 04 48.12	-30 03 08	9.51	8.71	8.44	212.32±1.30	29.06.06	2x2700	Flames-UVES	19
								212.57±1.36	01.07.06	2x2700	Flames-UVES	
								213.31±1.30	19.07.06	2x2700	Flames-UVES	
(15)	62	2MASS 18044578-3002470	18 04 45.79	-30 02 47	11.30	10.49	10.34	212.84±0.49	29.06.06	2x2700	Flames-UVES	43
								213.10±0.37	01.07.06	2x2700	Flames-UVES	
								213.16±0.37	19.07.06	2x2700	Flames-UVES	
(16)	63	2MASS 18044537-3003468	18 04 45.36	-30 03 46	11.32	10.63	10.41	209.18±0.26	29.06.06	2x2700	Flames-UVES	35
								209.41±0.30	31.05.06	2x2700	Flames-UVES	
(17)	64	2MASS 18044775-3003469	18 04 47.75	-30 03 47	12.16	11.48	11.33	214.69±0.60	29.06.06	2x2700	Flames-UVES	38
								214.77±0.47	01.07.06	2x2700	Flames-UVES	
								214.92±0.31	19.07.06	2x2700	Flames-UVES	
(18)	65	2MASS 18044890-3003472	18 04 48.90	-30 03 47	12.03	11.25	11.22	205.08±0.26	29.06.06	2x2700	Flames-UVES	57
								205.29±0.23	31.05.06	2x2700	Flames-UVES	
(19)	66	2MASS 18044963-3003382	18 04 49.61	-30 03 37	9.17	8.43	8.20	215.16±1.74	26.05.06	3x2700	Flames-UVES	23
								216.25±1.14	19.07.06	3x2700	Flames-UVES	
								214.70±1.36	20.07.06	2x2700	Flames-UVES	
								216.08±1.14	27.07.06	2x2700	Flames-UVES	
(20)	68	2MASS 18045165-3003232	18 04 51.64	-30 03 23	10.32	9.47	9.27	202.52±0.57	29.06.06	2x2700	Flames-UVES	18
								203.38±0.54	31.05.06	2x2700	Flames-UVES	
(21)	69	2MASS 18045116-3003150	18 04 51.16	-30 03 14	11.68	10.98	10.88	218.26±0.52	29.06.06	2x2700	Flames-UVES	39
								218.31±0.53	01.07.06	2x2700	Flames-UVES	
								218.17±0.44	19.07.06	2x2700	Flames-UVES	
(22)	70	2MASS 18045136-3003047	18 04 51.36	-30 03 04	10.86	10.09	9.90	216.06±0.63	29.06.06	2x2700	Flames-UVES	26
								215.82±0.45	31.05.06	2x2700	Flames-UVES	
(23)	71	2MASS 18045042-3002591	18 04 50.46	-30 03 00	13.53	13.03	12.94	205.57±0.31	26.05.06	3x2700	Flames-UVES	36
								205.80±0.49	19.07.06	3x2700	Flames-UVES	
								205.62±0.31	20.07.06	2x2700	Flames-UVES	
(24)	72	VVV J180443.90-300344.38	18 04 43.89	-30 03 44	13.83	13.34	13.21	205.63±0.32	27.07.06	2x2700	Flames-UVES	25
								-16.33±0.49	26.05.06	3x2700	Flames-UVES	
								-16.75±0.38	19.07.06	3x2700	Flames-UVES	
								-16.64±0.36	20.07.06	2x2700	Flames-UVES	
								-16.81±0.31	27.07.06	2x2700	Flames-UVES	
(25)	73	2MASS 18044544-3004174	18 04 45.44	-30 04 17	13.62	13.11	12.99	209.43±0.34	26.05.06	3x2700	Flames-UVES	30
								209.53±0.57	19.07.06	3x2700	Flames-UVES	
								209.23±0.60	20.07.06	2x2700	Flames-UVES	
								208.95±0.42	27.07.06	2x2700	Flames-UVES	
(26)	75	2MASS 18045025-3004211	18 04 50.25	-30 04 21	12.41	11.76	11.56	112.47±0.24	26.05.06	3x2700	Flames-UVES	38
								112.35±0.36	19.07.06	3x2700	Flames-UVES	
								112.57±0.35	20.07.06	2x2700	Flames-UVES	
								112.29±0.26	27.07.06	2x2700	Flames-UVES	
(27)	76	2MASS 18045282-3004331	18 04 52.81	-30 04 33	13.40	12.85	12.70	115.82±0.24	26.05.06	3x2700	Flames-UVES	25
								115.58±0.49	19.07.06	3x2700	Flames-UVES	
								115.60±0.37	20.07.06	2x2700	Flames-UVES	
								115.49±0.31	27.07.06	2x2700	Flames-UVES	
(28)	80	VVV J180446.26-300200.99	18 04 46.26	-30 02 00	14.05	13.53	13.46	214.22±0.37	26.05.06	3x2700	Flames-UVES	25
								213.99±0.76	19.07.06	3x2700	Flames-UVES	
								214.87±0.88	20.07.06	2x2700	Flames-UVES	
								213.77±0.41	27.07.06	2x2700	Flames-UVES	
(29)	82	2MASS 18045450-3003063	18 04 54.50	-30 03 06	13.05	12.51	12.37	-106.31±0.27	29.06.06	2x2700	Flames-UVES	22
								-106.36±0.28	01.07.06	2x2700	Flames-UVES	
								-105.86±0.43	19.07.06	2x2700	Flames-UVES	
(30)	83	2MASS 18044436-3003051	18 04 44.36	-30 03 05	13.37	12.85	12.77	140.23±0.43	29.06.06	2x2700	Flames-UVES	49
								139.66±0.49	01.07.06	2x2700	Flames-UVES	
								140.06±0.73	19.07.06	2x2700	Flames-UVES	
(31)	84	2MASS 18045102-3004227	18 04 51.02	-30 04 22	10.34	9.52	9.309	-113.85±0.62	29.06.06	2x2700	Flames-UVES	15
								-113.75±0.63	01.07.06	2x2700	Flames-UVES	
								-113.41±0.59	19.07.06	2x2700	Flames-UVES	
(32)	86	2MASS 18045165-3004389	18 04 51.64	-30 04 39	10.68	9.89	9.08	-122.46±0.30	29.06.06	2x2700	Flames-UVES	16

Table 2. continued.

#	Obj.	ID	R.A.	DEC	J_0^a (mag)	H_0^a (mag)	$K_{s,0}^a$ (mag)	v_r (km s ⁻¹)	Date	Exp. (s)	Instrument	(S/N)/px ^b
								-121.82±0.47	31.05.06	2x2700	Flames-UVES	
(33)	3014 ^c	2MASS 18044744-3003432	18 04 47.38	-30 03 43	13.49	13.01	12.88	212.00±2.50	15.08.99	3x1200	HIRES	34
(34)	3025 ^c	VVV J180447.67-300335.85	18 04 47.62	-30 03 36	13.51	12.98	12.90	216.80±1.50	02.06.00	6x1200	HIRES	34

Notes. The first column provides the number that we use to identify the stars in the finding chart (see below). The names of the targets used in the fits-headers of original observations are given in the second column. This enables for a better traceability when comparing with papers that have published analyses of some of these stars. These names are also short-hand names and will be used in the text. We also list VVV and 2MASS identifications (when available) in column 3 as well as the coordinates in column 4 and 5. De-reddened magnitudes and measured radial velocity are given from column 6 to 9. Some observation informations, such as date, exposures time, and instrument, are shown from column 10 to 12. In the last column, S/N measured from the spectrum is also included. ^a De-reddened magnitudes have been derived adopting the reddening law by Cardelli et al. (1989). ^b Signal-to-noise ratio of the final co-added spectrum. ^c The radial velocity is adopted from Carretta et al. (2001). The last column gives the S/N. The average S/N of the final co-added spectrum for each star was estimated using the *SPLOT* task within IRAF at three short wavelength regions (574.4 – 574.7 nm, 604.7 – 606.3 nm, and 606.8 – 607.6 nm).

Appendix A: NGC 6528 – a finding chart

Figure A.1 shows a finding chart centred on the field of the globular cluster NGC 6528. All stars from Table 2 are marked (two stars fall outside the image) and identified by the number that is listed in the first column in Table 2. The image is based on WFC3 observations with the HST and has been retrieved from the Mikulski Archive for Space Telescopes ⁷.

Appendix B: Linelist

This section presents the full linelist used in the study of the ten *Gaia* benchmark stars and the red giant branch stars in NGC 6528. The data is shown in Table B.1, where also references to the original sources of the data are given. Most of the lines have been included in the linelist used in the *Gaia*-ESO Survey (Gilmore et al. 2012, and Heiter et al., in prep.).

In the fourth column in Table B.1 we give the classification used in the *Gaia*-ESO linelist. Two flags are given, the left refers to the quality of the log *gf* and the second to the blending properties of the line.

- The flags have the following meaning for log *gf*:
 - y – Data come from a trusted source (mainly laboratory measurements with excellent accuracy).
 - u – Quality of data is not decided (advanced theoretical calculations and lower accuracy laboratory data).
 - n – Data are expected to have low accuracy.
- The flags have the following meaning for blending properties as assessed in spectra of the Sun and Arcturus:
 - y – Line is particularly un-blended or only blended with line of same species in both stars.
 - u – Line may be inappropriate in at least one of the stars.
 - n – Line is strongly blended with line(s) of different species in both the Sun and Arcturus.

⁷ <http://archive.stsci.edu/>

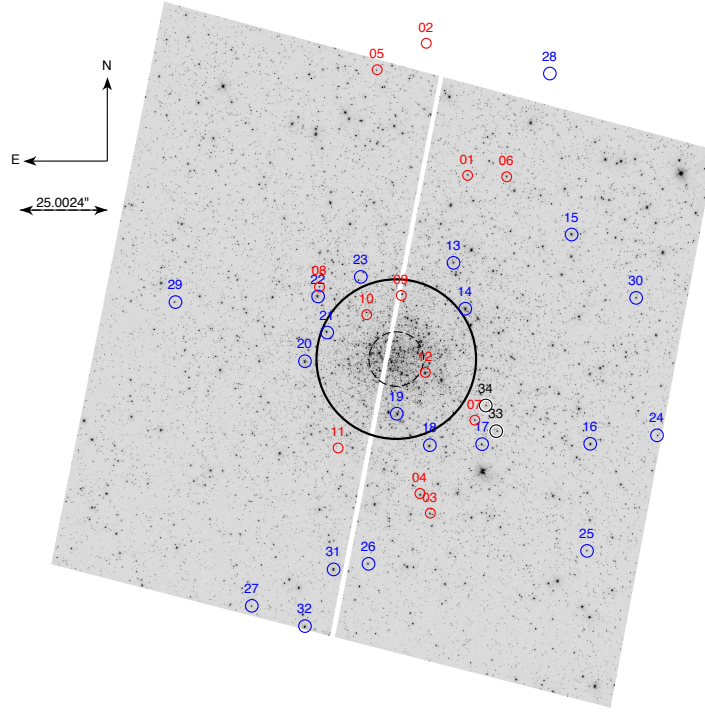


Fig. A.1. An image of the globular cluster NGC 6528 with the positions of stars we have analysed in this study marked. The stars are identified by the numbers listed in the first column in Table 2. Red circles show stars observed with UVES, blue circles show stars observed with FLAMES-UVES, and black circles show stars observed with HIRES. The numbers next to the circles refer to the numbers in Table 2. The core radius of the cluster (0.13 arcmin) is indicated by a red dashed line and the half-light (0.38 arcmin) by a black solid line. Data taken from Harris (1996). The image has been smoothed with a Gaussian to roughly mimic the seeing at Paranal.

Table B.1. Atomic line data.

λ (Å)	χ (eV)	$\log gf$	Flag	Ref.
H I				
6562.797	10.1990	0.710		(4)
Ca I				
6122.217	1.8860	-0.380	yy	(1)
6161.297	2.5230	-1.266	yn	(2)
6162.173	1.8990	-0.170		(1)
6166.439	2.5210	-1.142	yy	(2)
6169.042	2.5230	-0.797	yy	(2)
6169.563	2.5260	-0.478	yy	(2)
6439.075	2.5260	0.390	yy	(2)
6455.598	2.5230	-1.320	yy	(2)
Fe I				
4787.827	2.9980	-2.620	yu	(3)
4788.757	3.2370	-1.763	yu	(4)
4802.880	3.6420	-1.514	yy	(5)
4808.148	3.2510	-2.630	yy	(6)
4843.143	3.3970	-1.650		(3)
4882.143	3.4170	-1.480	nu	(3)
4910.017	3.3970	-1.280		(3)
4950.106	3.4170	-1.500	uy	(3)

Table B.1. continued.

λ (Å)	χ (eV)	$\log gf$	Flag	Ref.
4962.572	4.1780	-1.182	yu	(7)
4994.129	0.9150	-3.002	yy	(7)
5141.739	2.4240	-2.125	yy	(6)
5223.183	3.6350	-2.252	uy	(6)
5228.376	4.2200	-1.095	uu	(6)
5242.491	3.6340	-0.967	yy	(7)
5243.776	4.2560	-1.022	uu	(6)
5247.050	0.0870	-4.975	yu	(7)
5253.462	3.2830	-1.580	yu	(3)
5295.312	4.4150	-1.518	uy	(6)
5322.041	2.2790	-2.802	yy	(7)
5379.574	3.6940	-1.514	yy	(7)
5386.333	4.1540	-1.670	uy	(7)
5389.479	4.4150	-0.534	uy	(6)
5398.279	4.4450	-0.630	uy	(7)
5464.280	4.1430	-1.595	yy	(6)
5466.396	4.3710	-0.630	uu	(7)
5483.099	4.1540	-1.390	yu	(3)
5522.446	4.2090	-1.419	uy	(6)
5543.936	4.2170	-1.040	uy	(7)
5546.506	4.3710	-1.124	yy	(6)
5560.212	4.4340	-1.090	yy	(7)
5618.632	4.2090	-1.250	yy	(3)
5633.947	4.9910	-0.230	uu	(7)
5636.696	3.6400	-2.511	uy	(6)
5638.262	4.2200	-0.770	uy	(7)
5651.469	4.4730	-1.763	uy	(6)
5653.865	4.3870	-1.402	uy	(6)
5661.346	4.2840	-1.756	yu	(7)
5662.516	4.1780	-0.410	yy	(3)
5679.023	4.6520	-0.756	yy	(6)
5701.544	2.5590	-2.160	yy	(7)
5705.465	4.3010	-1.355	yy	(7)
5731.762	4.2560	-1.200	yy	(7)
5741.848	4.2560	-1.672	yy	(7)
5775.081	4.2200	-1.080	yy	(3)
5778.453	2.5880	-3.430	yy	(7)
5793.915	4.2200	-1.622	uy	(6)
5811.914	4.1430	-2.333	uy	(6)
5814.807	4.2830	-1.820	uy	(6)
5855.077	4.6080	-1.478	yy	(7)
5859.586	4.5490	-0.419	ny	(7)
5861.110	4.2830	-2.450	ny	(4)
5862.356	4.5490	-0.127	ny	(7)
5902.473	4.5930	-1.797	uy	(6)
5905.672	4.6520	-0.690	yy	(7)
5916.247	2.4530	-2.914	yy	(7)
5927.789	4.6520	-1.090	uy	(4)
5929.676	4.5490	-1.211	uy	(6)
5930.180	4.6520	-0.230	uy	(7)
5934.655	3.9280	-1.170	uu	(4)
5956.694	0.8590	-4.553	yy	(7)
6027.051	4.0760	-1.089	yy	(7)
6056.005	4.7330	-0.489	uy	(6)
6065.482	2.6080	-1.470	yy	(7)
6079.008	4.6520	-1.020	uy	(7)
6094.373	4.6520	-1.566	uy	(6)
6096.664	3.9840	-1.776	uy	(6)
6151.618	2.1760	-3.299	yy	(4)
6165.360	4.1430	-1.474	yy	(4)

Table B.1. continued.

λ (Å)	χ (eV)	$\log gf$	Flag	Ref.
6173.336	2.2230	-2.880	yy	(7)
6187.989	3.9430	-1.620	uy	(7)
6200.313	2.6090	-2.405	yu	(7)
6213.430	2.2230	-2.482	yy	(4)
6226.736	3.8840	-2.120	uy	(7)
6240.646	2.2230	-3.233	yy	(4)
6270.225	2.8580	-2.573	yu	(6)
6297.793	2.2230	-2.702	yy	(7)
6315.811	4.0760	-1.610	yy	(7)
6322.685	2.5880	-2.426	yy	(4)
6481.870	2.2790	-2.984	yy	(4)
6609.110	2.5590	-2.632	yu	(6)
6627.544	4.5490	-1.475	uy	(6)
6699.142	4.5930	-2.101	yy	(7)
6705.101	4.6070	-1.057	ny	(6)
6713.743	4.7960	-1.425	uy	(6)
6739.522	1.5570	-4.794	yy	(7)
6750.153	2.4240	-2.604	yy	(7)
6810.262	4.6070	-0.986	yy	(4)
6828.591	4.6380	-0.820	yy	(7)
6842.685	4.6380	-1.169	uy	(6)
6843.655	4.5490	-0.830	yy	(7)
Fe II				
4993.358	2.8070	-3.684	yy	(8)
5197.568	3.2300	-2.293	yu	(6)
5234.625	3.2210	-2.280	yy	(9)
5264.812	3.2300	-3.130	yy	(9)
5325.553	3.2210	-3.320	yy	(10)
5337.722	3.2300	-3.338	yn	(6)
5414.073	3.2210	-3.580	yy	(9)
5425.257	3.1990	-3.390	yy	(10)
5991.376	3.1530	-3.650	uy	(10)
6084.111	3.1990	-3.881	uy	(10)
6149.246	3.8890	-2.719	uu	(6)
6247.557	3.8920	-2.430	uu	(10)
6369.462	2.8910	-4.230	yu	(10)
6432.680	2.8910	-3.570	yy	(10)
6456.383	3.9030	-2.190	uy	(10)
6516.077	2.8910	-3.279	yu	(6)

Notes. (1) Aldenius et al. (2009); (2) Smith & Raggett (1981); (3) Den Hartog et al. (2014); (4) VALD; (5) XXXO'Brian 1991; (6) Tsantaki et al. (2013); (7) *Gaia*-ESO Survey linelist; (8) Raassen & Uylings (1998); (9) Meléndez & Barbuy (2009); (10) Bensby et al. (2003).

Appendix C: Fitting of the wings of the $H\alpha$ line to derive T_{eff}

In this study we have fitted the wings of the $H\alpha$ line by eye. We chose this approach in order to gain a deeper understanding of the issues facing the analysis of this line in the spectra of metal-rich giant stars. However, for larger samples and for a more routine approach an automated method should be attempted.

Figure C.1 shows our fits for three benchmark stars with different T_{eff} (see the Figure caption). The warmest star is shown on top. This figure nicely illustrates the fact that the wings of the $H\alpha$ line get less and less well developed in stars with cooler and cooler temperatures. Eventually, the wings become sufficiently weak that it is impossible to determine T_{eff} from them.

Automated routines for fitting the wings should ideally be used. This is not yet well explored for metal-rich stars such as those in NGC 6528. Methods such as those in Barklem et al. (2002) should be possible to be adapted but it might become increasingly difficult to define suitable windows to fit the spectra in metal-rich red giant stars. Figure C.1 shows the fits for three of the benchmark stars. As we are doing the fits by hand we have been able to customise the fitting regions. An experienced researcher may decide on different windows for the different spectra (as in our case). However, it would be feasible to stick to a single set of windows with these high quality spectra. This is more difficult when the spectra have low S/N. Figure C.2 shows how difficult it is to find clean regions in spectra with relatively low S/N. The spectrum shown in the top panel has a S/N of 29 and the one in the bottom panel has a S/N of 46. The two stars both have $T_{\text{eff}} > 4400$ K, i.e. we would expect to be able to fit the $H\alpha$ line for both stars.

Appendix D: Surface gravity from the three Ca I lines at 612.22, 616.22, and 643.91 nm

In Method 2 and Modified Method 2 (Sect. 4.3.2) we fit the three strong Ca I lines at 612.22, 616.22, and 643.91 nm simultaneously to determine $\log g$. This is not necessarily the only way to make use of the gravity sensitivity of these three lines. For example, it would be possible to fit each of the lines individually and take the average of the three determinations. Such an approach would also offer the possibility to derive the scatter around the mean value as well as the error in the mean. In Table D.1 we report such results for the ten benchmark stars we have studied.

We found that for most stars, the typical uncertainty is around 0.10 dex. But, the determined $\log g$ suffers from a larger uncertainty for a lower gravity star. Except for βAra , the average of the three measured gravities ($\log g_{\text{ave}}$) agree well with the obtained gravity ($\log g_{\text{method2}}$) by fitting the three Ca lines simultaneously listed in Table D.1. It is clearly shown that the determined $\log g_{\text{method2}}$ is strongly weighted by the second Ca line as $\log g$ from the Ca I 616.2 nm line is much larger than the other two lines.

Appendix E: Exploration of impact of S/N on determination on stellar parameters for cool, metal-rich giant stars

As discussed in Sects. 4.5 and 5.2 the S/N of the spectra influences the results, at least for low S/N. This is one of the major findings of this study.

For several of the stars in NGC 6528 we have multiple exposures. This allows us to analyse spectra of different S/N for the

same star. Using Method 2 and Modified Method 2 we analysed the spectra of five stars (Star-05, -07, -62, -65 and -67, IDs as in Table 2). Figures 6 and E.1 show the results of our investigation. As a reference value we use the final parameters determined for each star, Table 4. The results shown for $[\text{Fe}/\text{H}]$ were used to create Fig. 6.

It is easily seen, as expected, that when we analyse spectra of lower and lower S/N the scatter increases for all three parameters. It is in particular acute for $\log g$ which blows up to a rather large error quickly as the S/N deteriorates.

For T_{eff} there is a marked increase in scatter and different stars appear, perhaps to behave in different ways. It is in particular interesting to compare and contrast star-62 and star-71. For star-71 (with T_{eff} of 4560 K, thus analysed with Method 2) we systematically underproduce T_{eff} when we go to lower S/N, while the opposite is true for star-62 (with T_{eff} of 3967 K, thus analysed with Modified Method 2). For T_{eff} there is thus a difference between Method 2 and Modified Method 2. We recall that Method 2 uses the wings of the $H\alpha$ line to obtain T_{eff} whilst Modified Method 2 uses excitation equilibrium of Fe I lines as the $H\alpha$ wings disappear. Figure E.1 shows the detailed results.

The results for $[\text{Fe}/\text{H}]$ are discussed in detail in the main body of the paper.

Table D.1. Surface gravities measured from the strong Ca I lines.

Name	Results from Method 2							
	$\log g_r$	$\log g_{\text{Method2}}$	$\log g_1$	$\log g_2$	$\log g_3$	$\log g_{\text{ave}}$	$\sigma_{\log g_{\text{ave}}}$	Error
μ Leo	2.51	2.51	2.61	2.61	2.41	2.54	0.09	0.05
HD107328	2.09	1.97	2.26	1.95	2.20	2.14	0.13	0.08
	—	2.00	2.18	1.98	2.19	2.11	0.10	0.06
β Gem	2.90	2.89	2.98	2.91	2.75	2.88	0.10	0.06
ϵ Vir	2.77	2.91	2.93	2.92	2.64	2.83	0.13	0.08
	—	2.85	2.93	2.87	2.70	2.83	0.10	0.06
ξ Hya	2.87	2.94	3.03	2.96	2.77	2.92	0.11	0.06
Results from Modified Method 2								
Arcturus	1.64	1.66	1.77	1.59	1.68	1.68	0.07	0.04
	—	1.61	1.77	1.56	1.55	1.63	0.10	0.06
α Cet	0.68	0.87	0.61	0.71	1.19	0.84	0.25	0.14
γ Sge	1.05	1.12	1.18	1.09	0.92	1.06	0.11	0.06
α Tau	1.11	1.09	1.13	0.99	0.80	0.97	0.13	0.08
	—	1.29	1.47	1.29	0.87	1.21	0.25	0.14
β Ara	1.05	2.05	1.02	2.05	1.02	1.36	0.48	0.28
	—	2.06	1.26	2.06	1.26	1.53	0.38	0.22

Notes. The first column gives the name of the star. The second column gives the recommended $\log g$. The third column gives the obtained gravity by fitting the three Ca lines simultaneously in Method 2, and Modified Method 2. $\log g$ determined from each of the Ca I lines are listed in columns 4 to 6. The average and standard deviation of the three values are given in column 7 and 8 and the error in the mean in column 9 ($\sigma/\sqrt{N_{\text{lines}}}$).

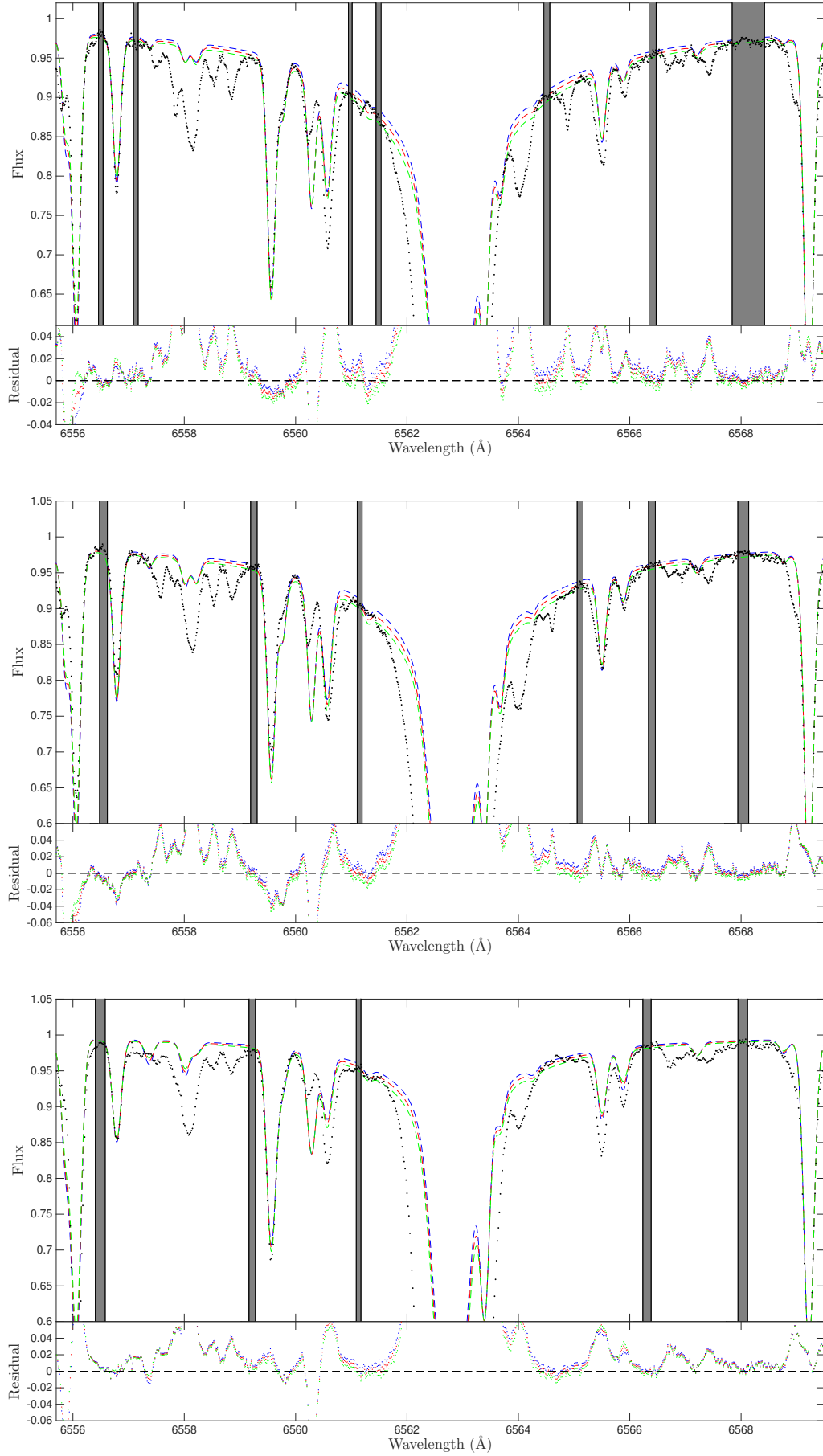


Fig. C.1. Comparison of synthetic spectra with the wings of H α for the *Gaia* benchmark star ϵ Vir ($T_{\text{eff}} = 5056$ K and $\log g = 2.8$ dex), ξ Hya ($T_{\text{eff}} = 4991$ K and $\log g = 2.96$), and HD 107328 ($T_{\text{eff}} = 4483$ K and $\log g = 2.0$ dex). The middle synthetic spectrum (in red colour) is the best fit to the H α wings, and the other two synthetic spectra indicate the shape of the wings when T_{eff} is changed according to our estimated uncertainty. The marked grey regions were used to evaluate the goodness of the fit. Note that these are relatively short since many of the spectra have very little clean "line continuum" thanks to the cool temperatures which results in many molecular lines being present in the spectra.

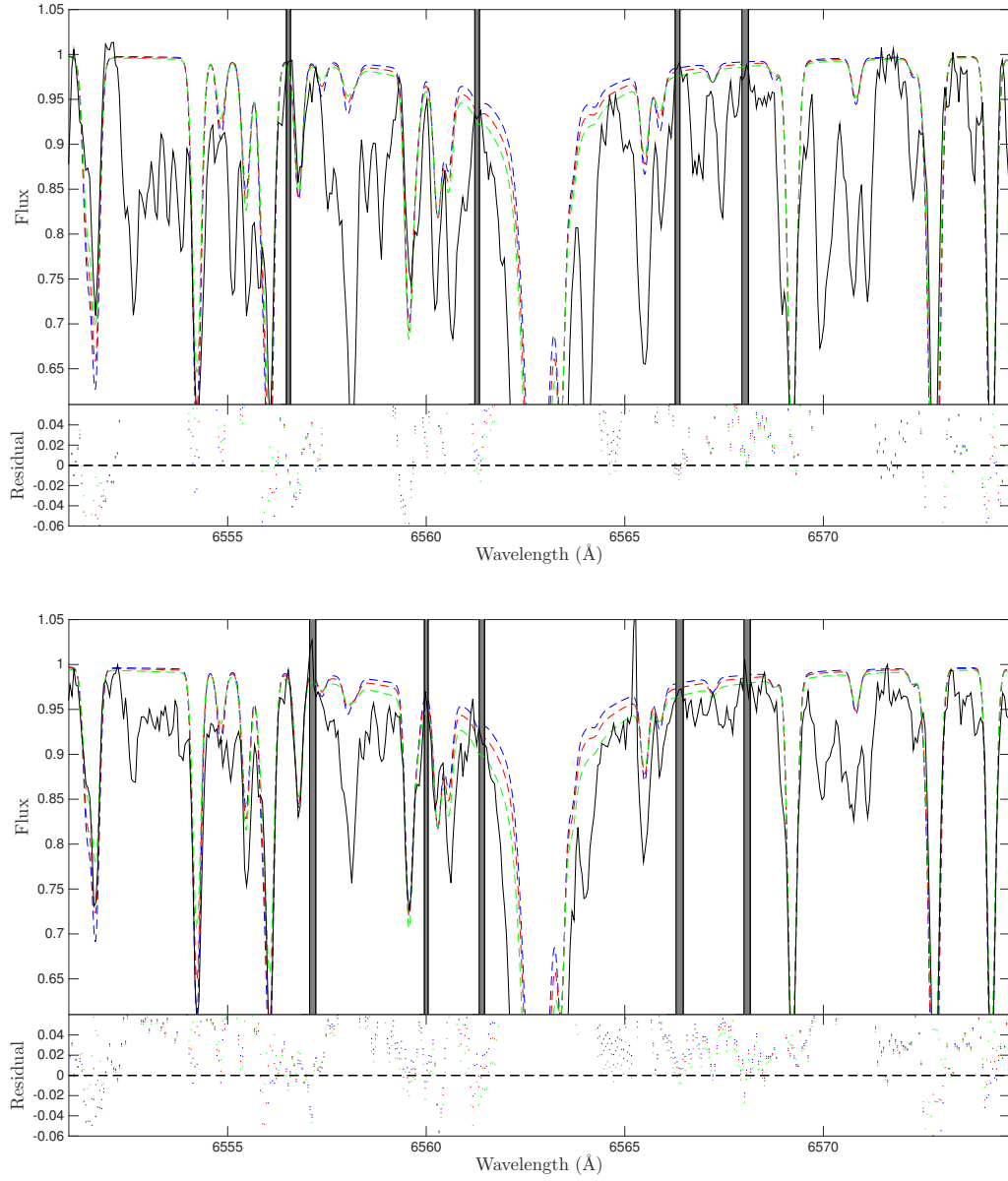


Fig. C.2. Comparison of synthetic spectra with the wings of H α two stars in NGC 6528. Star-06 ($T_{\text{eff}} = 4623$ K and $\log g = 1.98$ dex) and Star-07 ($T_{\text{eff}} = 4776$ K and $\log g = 2.50$ dex). The middle synthetic spectrum (in red colour) is the best fit to the H α wings, and the other two synthetic spectra indicate the shape of the wings when T_{eff} is changed according to our estimated uncertainty. The marked grey regions were used to evaluate the goodness of the fit. Note the richer and more noisy spectra for these stars as compared to the benchmark stars displayed in Fig. C.1.

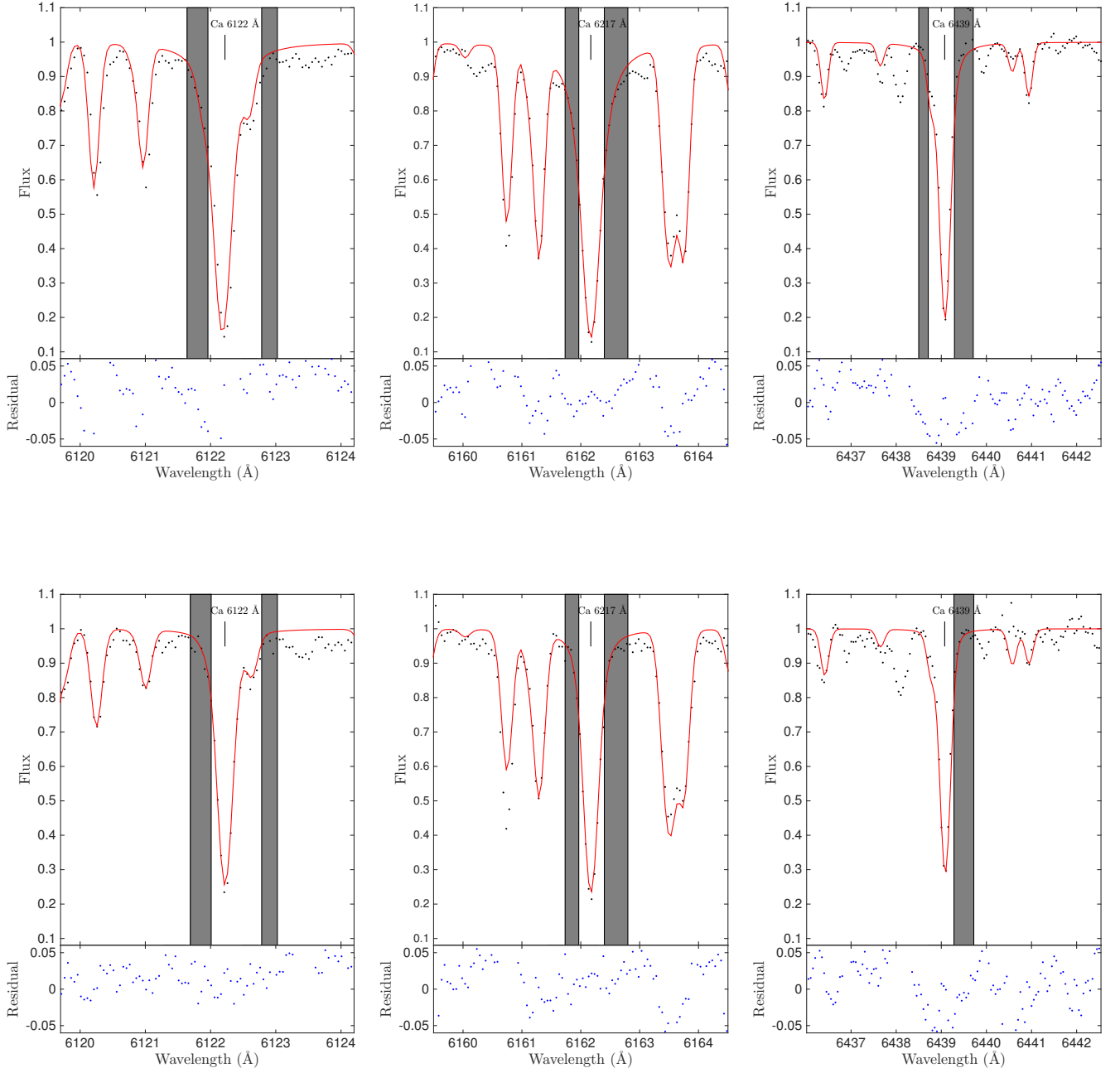


Fig. D.1. Comparison of synthetic spectra fitted to the wings of the three strong Ca I lines for two stars in NGC 6528. Star-05 ($T_{\text{eff}} = 4277$ K and $\log g = 1.95$ dex) and Star-07 ($T_{\text{eff}} = 4776$ K and $\log g = 2.50$ dex). The observed spectrum is shown as a dotted line. The fitted spectrum is shown in red. This is the best fit as evaluated inside SME using the exact regions indicated with grey shaded regions. All three lines are fitted simultaneously, as implemented in Method 2. In the lower panels the residuals are shown.

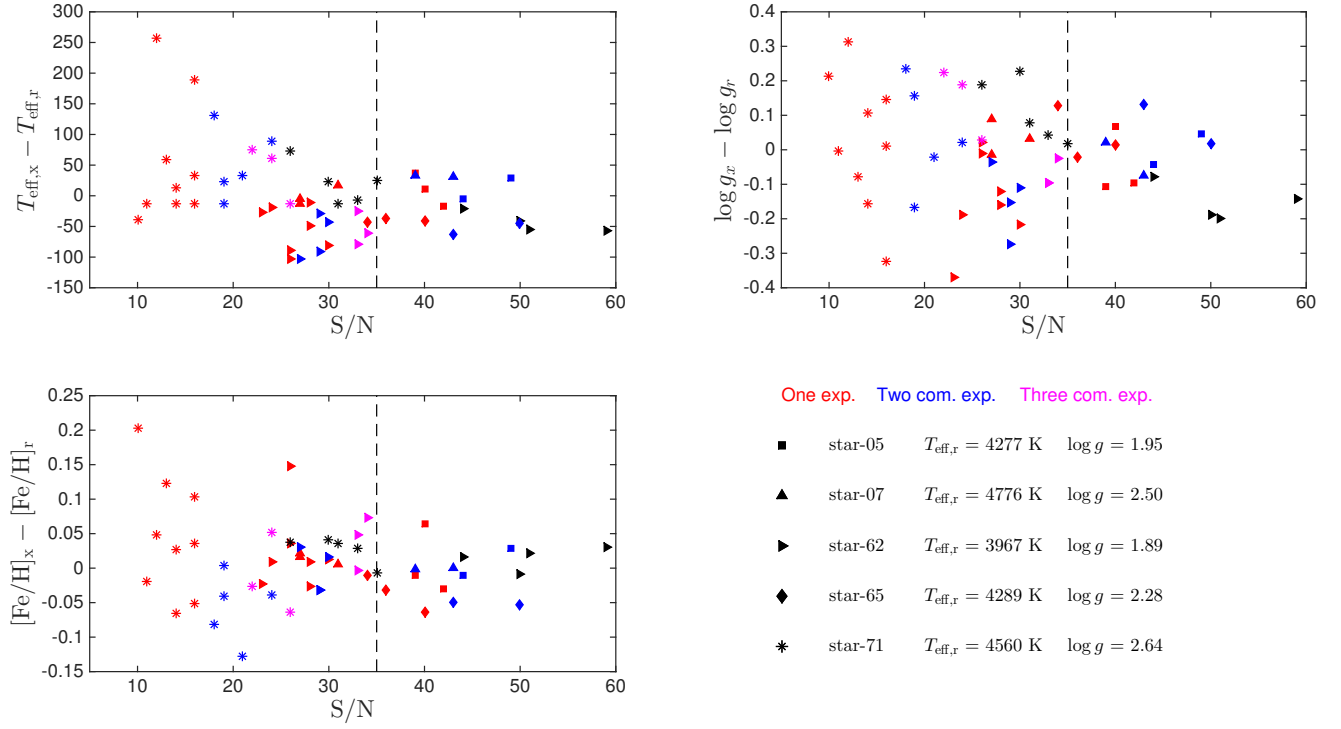


Fig. E.1. Comparison of the derived stellar parameters as a function of S/N. The y -axes show the difference between the value for each parameter derived from the low S/N spectrum and the value derived from the final combined spectrum (i.e., that used in the analysis in Sect. 6). The stellar parameters of the five stars are given in the legend. The colours refer to how many spectra have been combined to obtain the analysed spectrum (colours as indicated in the legend).